

NUMERICAL MODELLING OF
WAVEGUIDE INTERFACE

By

CLAYTON WEBSTER, B.SC.

A Thesis

Submitted to the School of Graduate Studies
in Partial Fulfillment of the Requirements
for the Degree
Master of Science

McMaster University

© Copyright by Clayton Webster, August 2003

MASTER OF SCIENCE (2003)

Department of Mathematics and Statistics
McMaster University
Hamilton, Ontario

TITLE: Numerical Modelling of Waveguide Interface

AUTHOR: Clayton Garrett Webster, B.Sc. (McMaster University)

SUPERVISOR: Professor Dimitry Pelinovsky

NUMBER OF PAGES: vii, 95

*To Gillian, Mom and Dad
for your love and guidance*

Abstract

We develop a computational algorithm for solving the stationary *Maxwell* equation at the interface between two planar waveguides. The algorithm operates with arbitrary refractive index profiles on both sides of the interface and with arbitrary incident electric field from one side. The algorithm computes the reflection and transmission coefficients for trapped waveguide modes, radiation waves and edge states localized at the interface.

We use spectral decompositions for one-dimensional *Schrodinger* operators and diagonalization of two symmetric matrices. By solving a set of linear equations at the interface between two waveguides, the numerical solution represents a full picture of electric and magnetic field distributions in each waveguide.

We also study absorbing layers in order to absorb outgoing waves from artificial boundary-reflected waveguides. By using a complexification of transverse space we introduce a thin absorbing layer on the boundaries of the computational domain.

Acknowledgements

I would like to take this opportunity to express my gratitude towards Dr. Dimitry Pelinovsky and Dr. Walter Craig for introducing me to the subject of Computational Electromagnetics. Special thanks to my supervisor Dimitry Pelinovsky for his many helpful suggestions and infinite patience. I look forward to working together in the future.

I am very grateful to my parents for their love and support, and for providing me with a place of tranquility all these years. Though it may have appeared that I would never move out of your home, I finally have. You have given me strength and wisdom and have been monumental throughout my educational career. As I move forward in the pursuit of my Ph.D in mathematics, I must thank you for helping me discover the gifts I have been given. Like a bird, I was born with wings but it was you who taught me how to fly.

Finally I wish to thank Gillian for helping me see that there is no sacrifice too great when you are putting all your powers into astounding results. Your encouragement and ability to help me remain motivated during the preparation of this document will be remembered always.

This research was generously supported by the Ontario Graduate Scholarship Program, my advisors and the Department of Mathematics at McMaster University.

”There must be a beginning of any great matter, but the continuing unto the end until it be thoroughly finished yields the true glory”, *Sir Francis Drake*

Table of Contents

Abstract	iv
Acknowledgements	v
Table of Contents	vi
Introduction	1
1 Equations for Planar Waveguides	5
1.1 The Stationary Maxwell Equation	5
1.2 The Stationary Schrodinger Equation	7
1.3 The Interface	8
1.4 Separation of Variables and Eigenvalue Problems	10
1.5 Energy Flux	13
2 Numerical Algorithm: Periodic Boundary Conditions	16
2.1 Introduction	16
2.2 Finite-Difference Frequency-Domain Method	17
2.3 Solving the System away from the Interface	19
2.4 Matching Conditions at the Interface	20
2.4.1 Left of the interface: $z < 0$	20
2.4.2 Right of the interface: $z > 0$	21
2.4.3 At the interface: $z = 0$	21
2.5 Solutions of the Interface Equations	22
2.6 The Conservation Law	24
2.7 Visualization of Particular Solutions	27
2.7.1 Varying ρ^+ , fixed q_0^+	28
2.7.2 Varying q_0^+ , fixed ρ^+	33

3	Numerical Algorithm with Absorbing Layers	39
3.1	Introduction	39
3.2	Complexification of Transverse Space	40
3.3	Finite-Difference Frequency-Domain Method	45
3.4	Solutions of the Interface Equations	48
3.5	Visualization of Particular Solutions	50
3.6	The Splitting Phenomena	58
4	Summary	62
	Appendix A: Numerical Code from Chapter 2	65
	Appendix B: Numerical Code from Chapter 3	82
	Bibliography	93

Introduction

Guided Waves. When an electromagnetic wave packet propagates through vacuum, it naturally diverges like a spherical wave, for it travels with equal speed in all directions [21]. The presence of material substance does however affect propagation of electromagnetic waves.

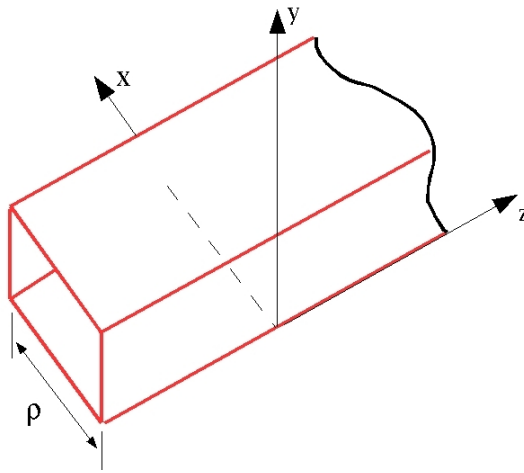


Figure 1. A three-dimensional planar waveguide of width ρ that guides electromagnetic waves propagating in the z direction.

A material medium that confines and guides a propagating electromagnetic wave is referred to as a waveguide. A planar waveguide¹ is an electromagnetic waveguide (a) that consists solely of dielectric materials, (b) in which the dielectric propagation

¹Their principle of operation is the same as that for optical fibers that are circular in cross section; that are used in fiber optic cables for long-distance transmission.

medium has a rectangular cross section, (c) that has a width, thickness, and refractive indices that determine the operating wavelength and the modes the guide will support beyond the equilibrium length, (d) that may be cladded, protected, distributed, and electronically controllable, and (e) that may be used in various applications, such as in integrated optical circuits (IOCs) [24]. An example of a typical three dimensional planar waveguide can be seen in Figure 1.

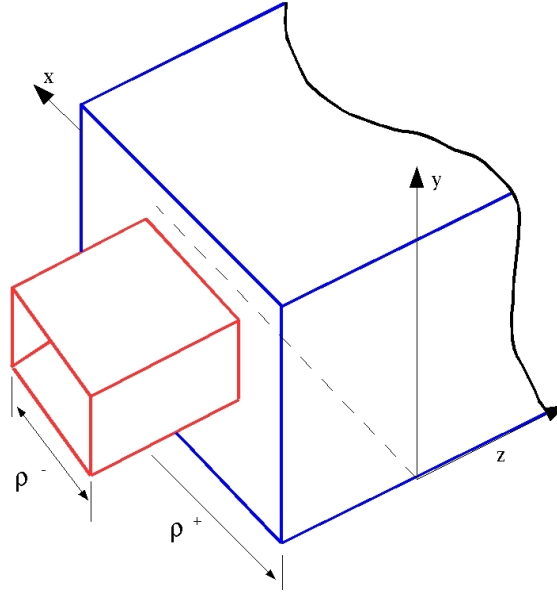


Figure 2. The interface between two three-dimensional planar waveguides of widths ρ^- and ρ^+ respectively that guide electromagnetic waves propagating in the z direction.

The purpose of this project is to develop a computational algorithm for solving the stationary *Maxwell* equation at the interface between two planar waveguides; as seen in Figure 2. The algorithm operates with arbitrary refractive index profiles on both sides of the interface and with arbitrary incident electric field from one side. The algorithm computes the reflection and transmission coefficients for trapped waveguide modes, radiation waves and edge states localized at the interface.

For many years, one of the most commonly used numerical methods for the simulation of electromagnetic wave propagation in planar waveguides, is the finite-difference time-domain (FDTD) method [18][23][26]. For solving interaction problems with the FDTD method, various techniques have been used in the past to absorb the outgoing waves, such as the matched layer [14] or the one-way approximation of the wave equation [7][12]. The most recent and widely used is the perfectly matched layer (PML) boundary conditions [3]. To be used with the FDTD method, the PML technique consists of surrounding a computational domain with a absorbing layer described in [3][4].

In this project, we describe a new technique for the simulation of electromagnetic wave propagation at the interface between two planar waveguides. By working in the frequency domain and using a procedure referred to as the finite-difference frequency-domain (FDFD) method, we reduce the electromagnetic wave propagation problem to spectral decompositions for one-dimensional *Schrodinger* operators and diagonalization of two symmetric matrices. In comparison with the FDTD method, the FDFD method requires less computation and storage, yet produces a convergent algorithm with accurate results. Our algorithm also has the ability to be implemented in parallel computations. The result of the FDFD method is a set of linear equations at the interface between two planar waveguides where the numerical solution represents a full picture of electric and magnetic field distributions in each waveguide. To absorb outgoing waves from artificial boundary-reflected waveguides, we modify the PML technique for the FDFD method. A complexification of transverse space will introduce a thin absorbing layer on the boundaries of the computational domain.

The project is described as follows. In chapter 1 we discuss the three-dimensional time-dependent *Maxwell's* equations. Using the *Fourier* transform and analysis of partial differential equations, we reduce them to a one-dimensional ordinary differential equation in the frequency domain. The numerical algorithm that solves the resulting one-dimensional propagation equation, using the FDFD method, is developed in chapter 2. To absorb outgoing waves from artificial boundary-reflected waveguides, chapter 3 describes a modification of the algorithm due to absorbing layers. The last sections of both chapter 2 and chapter 3 are devoted to numerical experiments in order to examine how the theoretical results are preserved in practical computations.

Chapter 1

Equations for Planar Waveguides

1.1 The Stationary Maxwell Equation

Propagation of electromagnetic waves in planar passive waveguides is governed by *Maxwell's* equations [17][25]. These equations are as follows

$$\nabla \times \mathbf{E} = -\frac{\partial \mathbf{B}}{\partial t}, \quad (1.1.1)$$

$$\nabla \times \mathbf{H} = \frac{\partial \mathbf{D}}{\partial t}, \quad (1.1.2)$$

$$\nabla \cdot \mathbf{D} = \nabla \cdot \mathbf{B} = 0 \quad (1.1.3)$$

where \mathbf{E} and \mathbf{H} are electric and magnetic field vectors, respectively, and \mathbf{D} and \mathbf{B} are corresponding electric and magnetic flux densities. The flux densities \mathbf{D} and \mathbf{B} arise in response to the electric field \mathbf{E} and magnetic field \mathbf{H} propagating inside the waveguide. They are expressed through the relations [2]

$$\mathbf{D} = \varepsilon_0 \mathbf{E} + \mathbf{P}, \quad (1.1.4)$$

$$\mathbf{B} = \mu_0 \mathbf{H}, \quad (1.1.5)$$

where ε_0 is the vacuum permittivity, μ_0 is the vacuum permeability, and \mathbf{P} is the induced electric polarization.

We reduce equations (1.1.1)-(1.1.5) to the wave equation for the electric field vector $\mathbf{E}(\mathbf{x}, t)$. By taking the curl of (1.1.1) while using (1.1.2) and (1.1.4) we obtain

$$\nabla \times \nabla \times \mathbf{E} = -\mu_0 \frac{\partial^2 \mathbf{D}}{\partial t^2} = \frac{-1}{c^2} \frac{\partial^2 \mathbf{E}}{\partial t^2} - \mu_0 \frac{\partial^2 \mathbf{P}}{\partial t^2} \quad (1.1.6)$$

where c is the speed of light in vacuum such that $c^2 = \frac{1}{\mu_0 \varepsilon_0}$. To complete the description, a relation between the induced polarization \mathbf{P} and the electric field \mathbf{E} is needed; which is taken in the general form [2]

$$\mathbf{P}(\mathbf{x}, t) = \varepsilon_0 \int_{-\infty}^{\infty} \chi^{(1)}(t - t') \cdot \mathbf{E}(\mathbf{x}, t') dt'. \quad (1.1.7)$$

We then see that

$$\mathbf{D}(\mathbf{x}, t) = \varepsilon_0 \left[\mathbf{E}(\mathbf{x}, t) + \int_{-\infty}^{\infty} \chi^{(1)}(\mathbf{x}, t - t') \cdot \mathbf{E}(\mathbf{x}, t') dt' \right]. \quad (1.1.8)$$

Since equations (1.1.6)-(1.1.7) are linear in \mathbf{E} , they can be written conveniently in the frequency domain. To do so, we must take advantage of the *Fourier* transform. We will use the following notation to denote the *Fourier* transform[9]

$$\mathbf{E}_\omega(\mathbf{x}, \omega) = \mathcal{F}[\mathbf{E}(\mathbf{x}, t)] = \int_{-\infty}^{\infty} \mathbf{E}(\mathbf{x}, t) e^{i\omega t} dt \quad (1.1.9)$$

where \mathbf{E}_ω is the *Fourier* transform of \mathbf{E} in the frequency domain. If $\mathbf{E}(\mathbf{x}, t)$ is a real-valued vector, then $\mathbf{E}_\omega(\mathbf{x}, \omega)$ is a complex-valued vector, such that $\overline{\mathbf{E}_\omega(\mathbf{x}, \omega)} = \mathbf{E}_\omega(\mathbf{x}, -\omega)$, where $\overline{\mathbf{E}_\omega}$ is the complex conjugate of \mathbf{E}_ω .

Then from (1.1.8), we see that

$$\begin{aligned}
\mathbf{D}_\omega(\mathbf{x}, \omega) &= \mathcal{F}[\mathbf{D}(\mathbf{x}, t)] = \mathcal{F}\left[\varepsilon_0 \left(\mathbf{E}(\mathbf{x}, t) + \int_{-\infty}^{\infty} \chi^{(1)}(\mathbf{x}, t - t') \cdot \mathbf{E}(\mathbf{x}, t') dt' \right)\right] \\
&= \varepsilon_0 \mathcal{F}[\mathbf{E}(\mathbf{x}, t)] + \varepsilon_0 \mathcal{F}\left[\int_{-\infty}^{\infty} \chi^{(1)}(\mathbf{x}, t - t') \cdot \mathbf{E}(\mathbf{x}, t') dt'\right] \\
&= \varepsilon_0 \mathcal{F}[\mathbf{E}(\mathbf{x}, t)] + \varepsilon_0 \mathcal{F}[\chi^{(1)}(\mathbf{x}, t)] \mathcal{F}[\mathbf{E}(\mathbf{x}, t)] \\
&= \varepsilon_0 \mathbf{E}_\omega(\mathbf{x}, \omega) (1 + \chi_\omega^{(1)}(\mathbf{x}, \omega))
\end{aligned} \tag{1.1.10}$$

where $\chi_\omega^{(1)}(\mathbf{x}, \omega)$ is the *Fourier* transform of $\chi^{(1)}(\mathbf{x}, t)$. From (1.1.10)

$$1 + \chi_\omega^{(1)}(\mathbf{x}, \omega) = n^2(\mathbf{x}, \omega), \tag{1.1.11}$$

is known as the the frequency-dependent dielectric constant. Recalling (1.1.6), we see from above that if

$$\nabla \times \nabla \times \mathbf{E} = -\mu_0 \frac{\partial^2 \mathbf{D}}{\partial t^2}$$

then

$$\nabla \times \nabla \times \mathbf{E}_\omega(\mathbf{x}, \omega) = \mu_0 \omega^2 \mathbf{D}_\omega(\mathbf{x}, \omega). \tag{1.1.12}$$

Therefore, in the frequency domain, we have arrived at the stationary *Maxwell* equation

$$\nabla \times \nabla \times \mathbf{E}_\omega(\mathbf{x}, \omega) - n^2(\mathbf{x}, \omega) \frac{\omega^2}{c^2} \mathbf{E}_\omega(\mathbf{x}, \omega) = 0. \tag{1.1.13}$$

1.2 The Stationary Schrodinger Equation

Until now there have been no assumptions on the dimension vector \mathbf{x} , which we will now elaborate on. We would like to consider a two-dimensional waveguide problem that is y -independent. That is, we will project onto the xz -plane such that $\mathbf{x} = (x, z)$.

A geometric configuration of our interface problem can be seen in Figure 1-1.

To further investigate (1.1.13), we define $\mathbf{E}_\omega = E_{\omega,x}\mathbf{i} + E_{\omega,y}\mathbf{j} + E_{\omega,z}\mathbf{k}$, where $E_{\omega,x}$, $E_{\omega,y}$ and $E_{\omega,z}$ depend on x , z and ω . Then we observe that

$$\begin{aligned} \nabla \times \nabla \times \mathbf{E}_\omega &= \left(-\frac{\partial^2}{\partial z^2} E_{\omega,x} + \frac{\partial^2}{\partial z \partial x} E_{\omega,z} \right) \mathbf{i} - \left(\frac{\partial^2}{\partial x^2} E_{\omega,y} + \frac{\partial^2}{\partial z^2} E_{\omega,y} \right) \mathbf{j} + \\ &+ \left(\frac{\partial^2}{\partial x \partial z} E_{\omega,x} - \frac{\partial^2}{\partial x^2} E_{\omega,z} \right) \mathbf{k}. \end{aligned} \quad (1.2.1)$$

By combining (1.2.1) and (1.1.13) we arrive at the following equations

$$-\frac{\partial^2}{\partial z^2} E_{\omega,x} + \frac{\partial^2}{\partial z \partial x} E_{\omega,z} = n^2(\mathbf{x}, \omega) \frac{\omega^2}{c^2} E_{\omega,x}, \quad (1.2.2)$$

$$-\frac{\partial^2}{\partial x^2} E_{\omega,y} - \frac{\partial^2}{\partial z^2} E_{\omega,y} = n^2(\mathbf{x}, \omega) \frac{\omega^2}{c^2} E_{\omega,y}, \quad (1.2.3)$$

$$\frac{\partial^2}{\partial x \partial z} E_{\omega,x} - \frac{\partial^2}{\partial z^2} E_{\omega,z} = n^2(\mathbf{x}, \omega) \frac{\omega^2}{c^2} E_{\omega,z}. \quad (1.2.4)$$

By looking above we see that (1.2.3) is dependant only on $E_{\omega,y}$ and, thus, $E_{\omega,y}$ is decoupled from $E_{\omega,x}$ and $E_{\omega,z}$. Whereas, (1.2.2) and (1.2.4) are coupled; dependant on both $E_{\omega,x}$ and $E_{\omega,z}$. This is no surprise since any solution to (1.1.13) is a linear superposition of TE (transverse electric) mode, $E_{\omega,y}\mathbf{j}$, and TM (transverse magnetic) mode, $E_{\omega,x}\mathbf{i} + E_{\omega,z}\mathbf{k}$ [4]. In the TE case, (1.2.3) can be rewritten as

$$\nabla^2 E_{\omega,y}(\mathbf{x}, \omega) + n^2(\mathbf{x}, \omega) \frac{\omega^2}{c^2} E_{\omega,y}(\mathbf{x}, \omega) = 0, \quad \mathbf{x} = (x, z), \quad (1.2.5)$$

which is known as the two-dimensional stationary *Schrodinger* equation.

1.3 The Interface

From this point further we will only be interested in the TE case. Only considering a single frequency $\omega = \omega_0$, we reformulate (1.2.5) as

$$\nabla^2 \Psi(x, z) + q(x, z) \Psi(x, z) = 0 \quad (1.3.1)$$

where

$$\Psi(x, z) = E_{\omega, y}(\mathbf{x}, \omega_0) \text{ and } q(x, z) = n^2(x, z) \frac{\omega_0^2}{c^2}. \quad (1.3.2)$$

The function $q(x, z)$ is a piecewise continuous quantum potential function of z for $z \geq 0$ and $z \leq 0$.

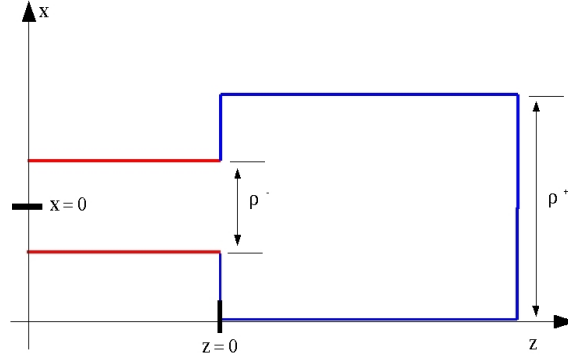


Figure 1-1. The interface configuration in the two-dimensional xz -plane of the two planar waveguides of widths ρ^- and ρ^+ .

As seen in Figure 1-1 the interface at $z = 0$ divides the plane \mathbb{R}^2 into two sub-domains D^- and D^+ . Such sub-domains corresponding to the left and right of the interface are respectively defined by

$$D^- = \{(x, z) \in \mathbb{R}^2 : z \leq 0\} \text{ and } D^+ = \{(x, z) \in \mathbb{R}^2 : z \geq 0\}.$$

The domains D^- and D^+ intersect at the line $z = 0$, which corresponds to the interface. Continuing in this manner we define

$$q(x, z) = \begin{cases} q^+(x), & \text{for } z \geq 0 \\ q^-(x), & \text{for } z \leq 0 \end{cases} \quad (1.3.3)$$

and

$$\Psi(x, z) = \begin{cases} \Psi^+(x, z), & \text{for } (x, z) \in D^+ \\ \Psi^-(x, z), & \text{for } (x, z) \in D^-. \end{cases} \quad (1.3.4)$$

We assume henceforth that $\lim_{|x| \rightarrow \infty} q^+(x) = q_\infty^+ > 0$ and $\lim_{|x| \rightarrow \infty} q^-(x) = q_\infty^- > 0$.

Furthermore, from (1.3.1) we now have two homogeneous partial differential equations:

$$\nabla^2 \Psi^+(x, z) + q^+(x) \Psi^+(x, z) = 0, \quad (x, z) \in D^+ \quad (1.3.5)$$

and

$$\nabla^2 \Psi^-(x, z) + q^-(x) \Psi^-(x, z) = 0, \quad (x, z) \in D^- \quad (1.3.6)$$

subject to the decaying boundary conditions:

$$\Psi^-, \Psi^+ \rightarrow 0 \text{ as } |x| \rightarrow \infty. \quad (1.3.7)$$

Due to the geometric configuration of our problem, we reduce the two-dimensional stationary *Schrodinger* equations, (1.3.5) and (1.3.6), to one-dimensional eigenvalue problems in the next section.

1.4 Separation of Variables and Eigenvalue Problems

In this section we discuss the method of separation of variables in applications to (1.3.5). Separating variables x and z , we look for particular solutions $\Psi^+(x, z) = \Psi_p^+(x, z)$ of (1.3.5) in the form

$$\Psi_p^+(x, z) = \Phi(x)\theta(z), \quad (1.4.1)$$

where we suppress the superscript for functions $\Phi(x)$ and $\theta(z)$, as well as for potential $q(x)$ to the right of the interface. A similar procedure can be developed for (1.3.6) to the left of the interface. Substituting $\Psi_p^+(x, z)$ into (1.3.5) we obtain

$$\frac{1}{\Phi(x)} \left(\frac{d^2}{dx^2} \Phi(x) + q(x) \Phi(x) \right) = -\frac{1}{\theta(z)} \left(\frac{d^2}{dz^2} \theta(z) \right). \quad (1.4.2)$$

Since x and z are independent, the left-hand-side and the right-hand-side of (1.4.2) must be constant in x and z . That is

$$\frac{d^2}{dz^2}\theta(z) + \lambda\theta(z) = 0 \quad (1.4.3)$$

and

$$\frac{d^2}{dx^2}\Phi(x) + q(x)\Phi(x) = \lambda\Phi(x) \quad (1.4.4)$$

where λ is a constant parameter.

The problem (1.4.4) defines the spectrum of the linear operator \mathcal{L} :

$$\mathcal{L} = \frac{d^2}{dx^2} + q(x) \quad (1.4.5)$$

on $L^2(\mathbb{R})$. The spectrum of \mathcal{L} consists of continuous, λ , and discrete, λ_j , eigenvalues which can be found by solving the following equations respectively [1]:

$$\mathcal{L}\Phi(x, \lambda) = \lambda\Phi(x, \lambda), \quad \lambda \in \mathbb{R} \quad (1.4.6)$$

and

$$\mathcal{L}\Phi_j(x) = \lambda_j\Phi_j(x), \quad j = 1, 2, \dots, m. \quad (1.4.7)$$

Since $\lim_{|x| \rightarrow \infty} |q(x)| = q_\infty$ and $q(x)$ is a compact potential, the continuous spectrum is located for [13][16]:

$$\mathcal{L}_C = \{\lambda \in \mathbb{R} : \lambda \leq q_\infty\}. \quad (1.4.8)$$

The discrete spectrum is finite-dimensional ($m < \infty$) and it is located for [13][16]:

$$\mathcal{L}_D = \{\lambda_j \in \mathbb{R} : q_\infty < \lambda_j < q_0, j = 1, 2, \dots, m\}, \quad (1.4.9)$$

where $q_0 = q(0)$.

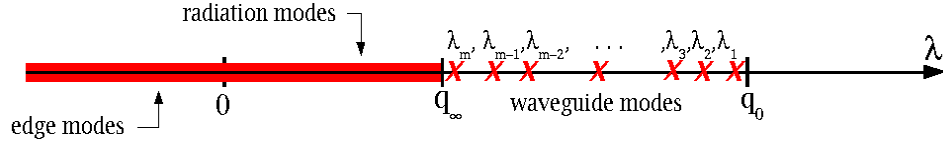


Figure 1-2. $sp(\mathcal{L})$: The spectrum of the operator \mathcal{L} consists of the edge modes, $\lambda < 0$, the radiation modes, $0 \leq \lambda \leq q_\infty$, and the waveguide modes $q_\infty < \lambda < q_0$.

Referring to Figure 1-2, we see that

$$\beta \equiv \sqrt{\lambda} = \begin{cases} \beta_R, & \text{if } \lambda = \{\lambda_j\}_{j=1}^m \text{ or } 0 \leq \lambda \leq q_\infty \\ i\beta_I, & \text{if } \lambda < 0. \end{cases} \quad (1.4.10)$$

Now we construct solutions to (1.4.3) with $\lambda = \beta^2$. Solving this equation we see that a general solution is defined by

$$\theta(z) = ce^{-i\beta z} + de^{i\beta z} \quad (1.4.11)$$

where c and d are arbitrary constants. With the use of the *Fourier* transform (1.1.9) we define

$$\theta(z, t) = \theta(z)e^{-i\omega_0 t} = ce^{-i(\beta z + \omega_0 t)} + de^{i(\beta z - \omega_0 t)}, \quad \omega_0 > 0 \quad (1.4.12)$$

which allows us to conclude that $ce^{-i\beta z}$ represents a wave moving from the right to the left while $de^{i\beta z}$ represents a wave moving from the left to the right. This brings us to the following general solution for (1.3.5) or (1.3.6)

$$\Psi(x, z) = \sum_{sp(\mathcal{L})} c_\lambda \Phi_\lambda(x) e^{-i\beta z} + \sum_{sp(\mathcal{L})} d_\lambda \Phi_\lambda(x) e^{i\beta z}, \quad (1.4.13)$$

where c_λ and d_λ are arbitrary constants, $\sum_{sp(\mathcal{L})} \equiv \sum_{j=1}^m + \int_{-\infty}^{q_\infty} d\lambda$, and $\Phi_\lambda(x)$ are eigenfunctions of the discrete and continuous spectrum of \mathcal{L} .

Following from (1.4.13) and the above discussion we can now describe the general solution to both (1.3.5) and (1.3.6). To the left of the interface:

$$\begin{aligned} \Psi^-(x, z) = & \sum_{j=1}^{m^-} c_j^- \Phi_j^-(x) e^{-i\beta_j^- z} + \int_{-\infty}^0 c^-(\lambda) \Phi^-(x, \lambda) e^{\beta_I^-(\lambda) z} d\lambda + \\ & + \int_0^{q_\infty^-} c^-(\lambda) \Phi^-(x, \lambda) e^{-i\beta_R^-(\lambda) z} d\lambda + \sum_{j=1}^{m^-} d_j^- \Phi_j^-(x) e^{i\beta_j^- z} \end{aligned} \quad (1.4.14)$$

where the last term represents the incident wave propagating from left to right and the first three terms represent the reflected wave propagating from right to left. We have set $d^-(\lambda) = 0$, assuming that the incident wave is superposed by trapped waveguide modes. To the right of the interface:

$$\begin{aligned} \Psi^+(x, z) = & \sum_{j=1}^{m^+} d_j^+ \Phi_j^+(x) e^{i\beta_j^+ z} + \int_{-\infty}^0 d^+(\lambda) \Phi^+(x, \lambda) e^{-\beta_I^+(\lambda) z} d\lambda + \\ & + \int_0^{q_\infty^+} d^+(\lambda) \Phi^+(x, \lambda) e^{i\beta_R^+(\lambda) z} d\lambda \end{aligned} \quad (1.4.15)$$

which defines the transmitted wave traveling from left to right. We call c_j^- and $c^-(\lambda)$ the reflected wave coefficients, d_j^+ and $d^+(\lambda)$ the transmitted wave coefficients and d_j^- is the incident wave coefficient.

1.5 Energy Flux

Here we consider the energy flux through the interface of two planar waveguides, given by *Poynting's* theorem¹. When the electromagnetic wave is periodic in time t with period T , the energy flux satisfies the balance equation [6][22]

$$\nabla \cdot \mathbf{S}_0 = 0, \quad (1.5.1)$$

¹John Henry Poynting (1852-1914).

where \mathbf{S}_0 is the time averaging *Poynting* vector defined as

$$\mathbf{S}_0 = \frac{1}{T} \int_0^T \mathbf{S}(\mathbf{x}, t) dt, \quad \mathbf{S} = \mathbf{E} \times \mathbf{H}. \quad (1.5.2)$$

The *Poynting* vector $\mathbf{S}(\mathbf{x}, t)$ represents the time-periodic energy flow through the dielectric material. Recall in the TE case that the electric and magnetic field vectors are defined respectively as

$$\mathbf{E}(\mathbf{x}, t) = E_y(\mathbf{x}, t)\mathbf{j} \text{ and } \mathbf{H}(\mathbf{x}, t) = H_x(\mathbf{x}, t)\mathbf{i} + H_z(\mathbf{x}, t)\mathbf{k} \quad (1.5.3)$$

then from (1.5.1)

$$\frac{\partial}{\partial x}(S_{0,x}) + \frac{\partial}{\partial z}(S_{0,z}) = 0. \quad (1.5.4)$$

Integrating (1.5.4) with respect to transverse variable x and using the decaying boundary conditions (1.3.7), we find that

$$\frac{\partial}{\partial z} \left[\int_{-\infty}^{\infty} (S_{0,z}) dx \right] = 0. \quad (1.5.5)$$

implying that

$$\int_{-\infty}^{\infty} (S_{0,z}) dx = C \quad (1.5.6)$$

where C is a constant in z . As a result, (1.5.6) defines the time-averaging energy flux, accumulative through the x -cross section, which remains constant along the z -interface. To further investigate this integral we must define E_y and H_x in the frequency domain. Using complex amplitudes and recalling that we are dealing with a single frequency ω_0 we define

$$E_y = \frac{1}{2\pi} [\Psi(x, z)e^{-i\omega_0 t} + \bar{\Psi}(x, z)e^{i\omega_0 t}] \quad (1.5.7)$$

and

$$H_x = \frac{1}{2\pi} [\Omega(x, z)e^{-i\omega_0 t} + \bar{\Omega}(x, z)e^{i\omega_0 t}]. \quad (1.5.8)$$

where $E_{\omega,y}(\mathbf{x}, \omega_0) = \Psi(x, z)$ as in (1.3.2) and $H_{\omega,x}(\mathbf{x}, \omega_0) = \Omega(x, z)$.

Using (1.5.3), (1.5.7) and (1.5.8), we express the energy flux $S_{0,z}$ as

$$S_{0,z} = \frac{1}{T} \int_0^T E_y H_x dt = \Psi \bar{\Omega} + \bar{\Psi} \Omega. \quad (1.5.9)$$

To express $S_{0,z}$ in terms of Ψ , we look for a relation between the electric field Ψ and the magnetic field Ω . We rewrite *Maxwell's* equations, specifically (1.1.1) and (1.1.5), for (1.5.3):

$$\frac{\partial E_y}{\partial z} = -\mu_0 \frac{\partial H_x}{\partial t}. \quad (1.5.10)$$

In the frequency domain, we use (1.5.7) and (1.5.8) to reduce (1.5.10) to the relation

$$\Omega = \frac{1}{i\mu_0\omega_0} \frac{\partial \Psi}{\partial z}. \quad (1.5.11)$$

The continuity of the electric field Ψ and magnetic field Ω at the interface $z = 0$ implies the following matching conditions at $z = 0$:

$$\Psi^-(x, 0) = \Psi^+(x, 0), \quad \frac{\partial \Psi^-}{\partial z}(x, 0) = \frac{\partial \Psi^+}{\partial z}(x, 0). \quad (1.5.12)$$

The *Poynting* theorem (1.5.6), with the use of (1.5.9) and Eq(1.5.12), reduces to the form

$$\begin{aligned} \int_{-\infty}^{\infty} (S_{0,z}) dx &= \langle \Omega, \Psi \rangle + \langle \Psi, \Omega \rangle \\ &= \frac{i}{\mu_0\omega_0} \left\langle \frac{\partial \Psi}{\partial z}, \Psi \right\rangle - \frac{i}{\mu_0\omega_0} \left\langle \Psi, \frac{\partial \Psi}{\partial z} \right\rangle \end{aligned} \quad (1.5.13)$$

where

$$\langle f, g \rangle = \int_{-\infty}^{\infty} \bar{f}(x, z) g(x, z) dx. \quad (1.5.14)$$

From (1.5.6) we conclude that (1.5.13) is constant in z and thus, constant across the interface.

Chapter 2

Numerical Algorithm: Periodic Boundary Conditions

2.1 Introduction

In this chapter we explore the Finite-Difference Frequency-Domain (FDFD) method to solve the spectral problem (1.4.4) for the one-dimensional *Schrodinger* operator. The spectral problem (1.4.4) has strictly real eigenvalues λ on the real axis $x \in \mathbb{R}$. The spectrum consists of isolated eigenvalues of the discrete spectrum and the continuous spectrum. We develop a numerical algorithm based on spectral decompositions for the one-dimensional *Schrodinger* operators, diagonalization formulae, and linear algebra solutions. By solving a set of linear equations at the interface between two planar waveguides, we construct the numerical solution which displays a full picture of electric and magnetic field distributions in each waveguide. Numerical approximations of reflected, incident and transmitted wave intensities are also found from the numerical solution.

2.2 Finite-Difference Frequency-Domain Method

The finite-difference approximation of the differential equation is obtained at a number of mesh points in the interval of integration thereby converting the differential equation to a set of simultaneous algebraic equations. The set of algebraic equations is linear (or nonlinear) if the differential equation is linear (or nonlinear).

After a separation of variables, discussed in the previous chapter, we are left with (1.4.4), solving for real eigenvalues λ :

$$\left[\frac{d^2}{dx^2} + q(x) \right] \Phi(x) = \lambda \Phi(x), \quad x \in \mathbb{R}. \quad (2.2.1)$$

This equation must be solved separately to the left and right of the interface, when $q = q^\pm(x)$ and $\Phi = \Phi^\pm(x)$.

We approximate the spectral problem, (2.2.1), on a finite interval $-M \leq x \leq M$, subject to the periodic boundary conditions:

$$\Phi(-M) = \Phi(M), \quad \Phi'(-M) = \Phi'(M). \quad (2.2.2)$$

The piecewise continuous quantum potential function $q(x)$ is defined by

$$q(x) = \begin{cases} q_\infty, & \text{for } |x| \geq \rho \\ q_0, & \text{for } |x| < \rho, \end{cases} \quad (2.2.3)$$

where ρ is the width of the corresponding waveguide. Hence q_∞ is the dielectric constant (refractive index) outside the waveguide and q_0 is the dielectric constant (refractive index) inside the waveguide.

To derive the finite-difference equations, from (2.2.1), the interval of integration $[-M, M]$ is divided into $2N$ equal parts of width $h = \frac{M - (-M)}{2N - 0} = \frac{2M}{2N} = \frac{M}{N}$. This implies that $x_0 = -M$ and $x_{2N} = M$ are the boundary mesh points, and

$$x_n = -M + nh, \quad n = 1, 2, \dots, (2N - 1)$$

are the interior mesh points. Let Φ_n denote a numerical approximation for $\Phi(x_n)$. We use the central difference formula for second derivative $\Phi''(x_n)$ [11]:

$$\Phi''(x_n) \approx \frac{\Phi_{n+1} + \Phi_{n-1} - 2\Phi_n}{h^2} + O(h^2). \quad (2.2.4)$$

When the truncation error is neglected, the finite-difference approximation of the above differential equation at $x = x_n$ is given by

$$\frac{\Phi_{n+1} + \Phi_{n-1} - 2\Phi_n}{h^2} + q_n \Phi_n = \lambda \Phi_n, \quad n = 1, 2, \dots, 2N - 1, 2N \quad (2.2.5)$$

where $q_n = q(x_n)$. Multiplying (2.2.5) by h^2 , we derive the linear system of equations

$$\Phi_{n+1} + \Phi_{n-1} + \Phi_n(h^2 q_n - 2) = \lambda h^2 \Phi_n, \quad n = 1, 2, \dots, 2N - 1, 2N. \quad (2.2.6)$$

It can be seen that Φ_0 appears on the left-hand side of (2.2.6) for $n = 1$ and Φ_{2N+1} appears on the left-hand side of the above equation for $n = 2N$. It follows from the periodic boundary conditions that $\Phi_0 = \Phi_{2N}$ and $\Phi_{2N+1} = \Phi_1$, such that the system given by (2.2.6) can be closed at $n = 1$ and $n = 2N$ with two equations:

$$\Phi_2 + \Phi_{2N} + \Phi_1(h^2 q_1 - 2) = \lambda h^2 \Phi_1 \quad (2.2.7)$$

$$\Phi_{2N-1} + \Phi_1 + \Phi_{2N}(h^2 q_{2N} - 2) = \lambda h^2 \Phi_{2N}. \quad (2.2.8)$$

Equations (2.2.6)-(2.2.8) represent a system of $2N$ equations in $2N$ unknowns $\Phi_1, \Phi_2, \dots, \Phi_{2N}$. Recalling that $q(x)$ is a known function of x then the coefficients of Φ_n can be computed. Thus, equations (2.2.6)-(2.2.8) can be solved by using numerical linear algebra. In fact, the above system can be expressed as a linear eigenvalue problem in the following form

$$A\Phi = \lambda h^2 \Phi \quad (2.2.9)$$

where

$$A = \begin{pmatrix} Q_1 & 1 & 0 & & \dots & 1 \\ 1 & Q_2 & 1 & 0 & \dots & 0 \\ 0 & 1 & Q_3 & 1 & 0 \dots & 0 \\ \vdots & & & \ddots & & \vdots \\ 0 & & \dots & 1 & Q_{2N-1} & 1 \\ 1 & 0 & \dots & 0 & 1 & Q_{2N} \end{pmatrix}, \Phi = \begin{pmatrix} \Phi_1 \\ \Phi_2 \\ \vdots \\ \Phi_{2N} \end{pmatrix}$$

and

$$Q_n = h^2 q_n - 2, \quad n = 1, 2, \dots, 2N.$$

We notice that the matrix A is symmetric; such that all eigenvalues λ are real-valued and the eigenvectors Φ are orthogonal for distinct eigenvalues λ [13].

2.3 Solving the System away from the Interface

Using (2.2.9) discussed in the previous section we arrive at the following eigenvalue problem to the left and right of the interface respectively:

$$A^- \Phi_j^- = \lambda_j^- h^2 \Phi_j^-, \quad j = 1, 2, \dots, 2N \quad (2.3.1)$$

and

$$A^+ \Phi_j^+ = \lambda_j^+ h^2 \Phi_j^+, \quad j = 1, 2, \dots, 2N. \quad (2.3.2)$$

Since A^\pm are symmetric matrices, they define two orthonormal bases for \mathbb{R}^{2N} consisting of eigenvectors $\{\Phi_j^\pm\}_{j=1}^{2N}$ with respect to the inner product:

$$\langle \mathbf{f}, \mathbf{g} \rangle = \sum_{j=1}^{2N} \bar{f}_j g_j \quad (2.3.3)$$

for all \mathbf{f} and \mathbf{g} . For each orthonormal basis of eigenvectors $\{\Phi_j^\pm\}_{j=1}^{2N}$, there exists a set of eigenvalues $\{\lambda_j^\pm\}_{j=1}^{2N}$ where $\lambda_j^\pm \in \mathbb{R}$. We arrive at the following orthogonal

diagonalization formulas:

$$D^- = Q_-^{-1} A^- Q_- = Q_-^T A^- Q_- = \text{diag}\{\lambda_1^-, \lambda_2^-, \dots, \lambda_{2N}^-\} \quad (2.3.4)$$

$$D^+ = Q_+^{-1} A^+ Q_+ = Q_+^T A^+ Q_+ = \text{diag}\{\lambda_1^+, \lambda_2^+, \dots, \lambda_{2N}^+\} \quad (2.3.5)$$

where Q_- and Q_+ are the $2N \times 2N$ matrices whose j th column is Φ_j^- and Φ_j^+ respectively. Hence we assume that the orthogonality relations

$$\langle \Phi_i^-, \Phi_j^- \rangle = \delta_{ij}, \quad \langle \Phi_i^+, \Phi_j^+ \rangle = \delta_{ij} \quad (2.3.6)$$

are satisfied for the respective orthonormal basis $\{\Phi_j^\pm\}_{j=1}^{2N}$.

2.4 Matching Conditions at the Interface

We now describe the spectral decomposition formulas for the systems on the left and right of the interface.

2.4.1 Left of the interface: $z < 0$

According to (1.4.14) and using (2.3.1), to construct the spectrum of the operator \mathcal{L} for $z < 0$, the FDFD method produces the following linear decomposition formula

$$\Psi^- = \sum_{j=1}^{2N} a_j \Phi_j^- e^{-i\beta_j^- z} + \sum_{j=1}^{2N} c_j \Phi_j^- e^{+i\beta_j^- z}, \quad \beta_j^- = \sqrt{\lambda_j^-}, \quad (2.4.1)$$

where the first sum corresponds to the reflected wave and the second sum corresponds to the incident wave. Therefore, a_j and c_j are referred to as the discretized reflected and incident wave coefficients for $j = 1, 2, \dots, 2N$. Since the incident wave is supposed to be a superposition of trapped waveguide modes of the discrete spectrum, we set $c_j = 0$ for all $\lambda_j^- \leq q_\infty^-$.

Some eigenvalues, λ_j^- , are positive and some eigenvalues, λ_j^- are negative. Hence, we order eigenvalues as: $\lambda_1^- \leq \lambda_2^- \leq \dots \leq \lambda_{N^-}^-$, where $\lambda_{N^-}^- < 0$, and $\lambda_{N^-+1}^- \leq \lambda_{N^-+2}^- \leq \dots \leq \lambda_{2N}^-$, where $\lambda_{N^-+1}^- \geq 0$. The negative eigenvalues correspond to edge modes, while the positive eigenvalues correspond to radiation and waveguide modes.

2.4.2 Right of the interface: $z > 0$

According to (1.4.14) and using (2.3.2) to construct the spectrum of the operator \mathcal{L} for $z > 0$, the FDFD method produces the following linear decomposition formula

$$\Psi^+ = \sum_{j=1}^{2N} b_j \Phi_j^+ e^{+i\beta_j^+ z}, \quad \beta_j^+ = \sqrt{\lambda_j^+}, \quad (2.4.2)$$

which corresponds to the transmitted wave. Therefore, b_j represents the discretized transmitted wave coefficients for $j = 1, 2, \dots, 2N$. Again, we order eigenvalues as $\lambda_1^+ \leq \lambda_2^+ \leq \dots \leq \lambda_{N^+}^+$, where $\lambda_{N^+}^+ < 0$, and $\lambda_{N^++1}^+ \leq \lambda_{N^++2}^+ \leq \dots \leq \lambda_{2N}^+$, where $\lambda_{N^++1}^+ \geq 0$.

2.4.3 At the interface: $z = 0$

At the interface, $z = 0$, we have the continuity equations given by (1.5.12) which yield a system of linear equations for coefficients a_j, b_j :

$$\sum_{j=1}^{2N} c_j \Phi_j^- + \sum_{j=1}^{2N} a_j \Phi_j^- = \sum_{j=1}^{2N} b_j \Phi_j^+ \quad (2.4.3)$$

$$\sum_{j=1}^{2N} \beta_j^- c_j \Phi_j^- - \sum_{j=1}^{2N} \beta_j^- a_j \Phi_j^- = \sum_{j=1}^{2N} \beta_j^+ b_j \Phi_j^+. \quad (2.4.4)$$

Equations (2.4.3) and (2.4.4) yield a system of $2N$ equations and $2N$ unknowns. The solution of the system for the reflected and transmitted wave coefficients, $\{a_j\}_{j=1}^{2N}$ and $\{b_j\}_{j=1}^{2N}$ is described in the next section.

2.5 Solutions of the Interface Equations

In order to solve the system of equations (2.4.3)-(2.4.4), we use projection operators P_k , associated with the eigenvector Φ_k^+ of the matrix A^+ :

$$P_k(\mathbf{f}) = \Phi_k^+ \langle \Phi_k^+, \mathbf{f} \rangle, \quad \mathbf{f} \in \mathbb{R}^{2N}, \quad k = 1, 2, \dots, 2N. \quad (2.5.1)$$

Applying the projection operator to (2.4.3), (2.4.4) and using the orthonormality conditions given by (2.3.6), we rewrite the system of linear equations (2.4.3)-(2.4.4) in the form:

$$\sum_{j=1}^{2N} c_j \langle \Phi_k^+, \Phi_j^- \rangle + \sum_{j=1}^{2N} a_j \langle \Phi_k^+, \Phi_j^- \rangle = b_k \quad (2.5.2)$$

$$\sum_{j=1}^{2N} \beta_j^- c_j \langle \Phi_k^+, \Phi_j^- \rangle - \sum_{j=1}^{2N} \beta_j^- a_j \langle \Phi_k^+, \Phi_j^- \rangle = \beta_k^+ b_k. \quad (2.5.3)$$

We solve this system for coefficients $\{a_j\}_{j=1}^{2N}$ and $\{b_j\}_{j=1}^{2N}$. Eliminating b_k from (2.5.2) and (2.5.3), we find that the coefficients $\{a_j\}_{j=1}^{2N}$ solve the linear system:

$$\sum_{j=1}^{2N} a_j (\beta_k^+ + \beta_j^-) \langle \Phi_k^+, \Phi_j^- \rangle = - \sum_{j=1}^{2N} c_j (\beta_k^+ - \beta_j^-) \langle \Phi_k^+, \Phi_j^- \rangle, \quad k = 1, 2, \dots, 2N. \quad (2.5.4)$$

To simplify the system, we use the matrix-vector form of (2.5.4):

$$B\mathbf{a} = \mathbf{g} \quad (2.5.5)$$

where B is a $2N \times 2N$ matrix defined by

$$B_{k,j} = (\beta_k^+ + \beta_j^-) \langle \Phi_k^+, \Phi_j^- \rangle, \quad j, k = 1, 2, \dots, 2N, \quad (2.5.6)$$

\mathbf{g} is $2N$ -dimensional vector written as

$$g_k = - \sum_{j=1}^{2N} c_j (\beta_k^+ - \beta_j^-) \langle \Phi_k^+, \Phi_j^- \rangle, \quad k = 1, 2, \dots, 2N, \quad (2.5.7)$$

and $\mathbf{a} = (a_1, a_2, \dots, a_{2N})^T$ is the vector of reflection coefficients. Following from (2.3.4) and (2.3.5), we can define

$$B = \sqrt{D^+} Q_+^T Q_- + Q_+^T Q_- \sqrt{D^-} \quad (2.5.8)$$

and

$$\mathbf{g} = - \left(\sqrt{D^+} Q_+^T Q_- - Q_+^T Q_- \sqrt{D^-} \right) \mathbf{c} \quad (2.5.9)$$

where $\mathbf{c} = (c_1, c_2, \dots, c_{2N})^T$ and $\sqrt{D^\pm}$ are diagonal matrices whose square are matrices D^\pm in equations (2.3.4)-(2.3.5).

An unique solution of (2.5.5) exists if and only if the matrix B is nonsingular. If B is singular, then the step size h must be modified. For example, if the waveguides are identical, i.e. $A^+ = A^-$, $\Phi_j^+ = \Phi_j^-$ and $\lambda_j^+ = \lambda_j^-$ for all $j = 1, 2, \dots, 2N$, then we see that

$$B_{k,j} = (\beta_k^+ + \beta_j^+) \langle \Phi_k^+, \Phi_j^+ \rangle = 2\beta_k^+ \delta_{kj}. \quad (2.5.10)$$

In this case, B becomes a singular matrix if $A^+ = A^-$ has a zero eigenvalue among the eigenvalues $\lambda_j^+ = \lambda_j^-$. When the step size h is modified, the eigenvalues λ_j^+ shift according to standard perturbation theory and the zero eigenvalue is removed. Hence, a small perturbation in h forces B to become nonsingular and, therefore, invertible, which allows us to solve (2.5.5). When B is nonsingular, a unique solution of (2.5.5) is defined by

$$\mathbf{a} = B^{-1} \mathbf{g}. \quad (2.5.11)$$

The solution (2.5.11) represents the entire set of reflection coefficients $\{a_j\}_{j=1}^{2N}$.

Using the set of reflection coefficients, $\{a_j\}_{j=1}^{2N}$, we can solve for the transmission

coefficients $\{b_j\}_{j=1}^{2N}$ in the vector $\mathbf{b} = (b_1, b_2, \dots, b_{2N})^T$. This is completed by representing (2.5.2) as the vector-matrix equation:

$$\mathbf{b} = E(\mathbf{a} + \mathbf{c}) \quad (2.5.12)$$

where

$$E_{k,j} = \langle \Phi_{\mathbf{k}}^+, \Phi_{\mathbf{j}}^- \rangle, \quad j, k = 1, 2, \dots, 2N. \quad (2.5.13)$$

Again, resulting from (2.3.4) and (2.3.5), we define $E = Q_+^T Q_-$.

Together with the vectors \mathbf{a} , \mathbf{b} and \mathbf{c} of reflected, transmitted and incident wave coefficients along with the spectrum of eigenvalues λ^\pm we recover, from equations (2.4.1) and (2.4.2), vector solutions $\Psi^-(z)$ and $\Psi^+(z)$ to the left and right of the interface $z = 0$. We combine these vector representations to construct plots of the entire surface $\Psi(x, z)$, showing transmission of light across the interface. Several plots are displayed in section 2.7.

2.6 The Conservation Law

Using *Poynting's* theorem, given by (1.5.13), we exploit conservation of incident, reflected and transmitted wave intensities across the interface. Using the trapezoidal rule and neglecting the global truncation error of order $O(h^2)$, we express the averaged energy flux in (1.5.13) to the left and right of the interface:

$$z < 0 : \quad \int_{-\infty}^{\infty} S_{0,z} dx \approx -\frac{i}{\mu_0 \omega_0} (P^- - \overline{P^-}) \quad (2.6.1)$$

and

$$z > 0 : \quad \int_{-\infty}^{\infty} S_{0,z} dx \approx -\frac{i}{\mu_0 \omega_0} (P^+ - \overline{P^+}) \quad (2.6.2)$$

where

$$P^- = \left\langle \Psi^-, \frac{d\Psi^-}{dz} \right\rangle, P^+ = \left\langle \Psi^+, \frac{d\Psi^+}{dz} \right\rangle \quad (2.6.3)$$

and the vector inner products are defined by (2.3.3).

From (2.6.1), to the left of the interface, we compute the inner product P^- as follows:

$$\begin{aligned}
P^- &= \sum_{j=1}^{2N} \sum_{k=1}^{2N} \left\langle \left(\bar{a}_j e^{i\beta_j^- z} + \bar{c}_j e^{-i\beta_j^- z} \right) \Phi_j^-, \left(-ia_k \beta_k^- e^{-i\beta_k^- z} + ic_k \beta_k^- e^{i\beta_k^- z} \right) \Phi_k^- \right\rangle \\
&= \sum_{j=1}^{2N} \sum_{k=1}^{2N} \left(-i\bar{a}_j a_k \beta_k^- e^{i\beta_j^- z - i\beta_k^- z} + i\bar{a}_j c_k \beta_k^- e^{i\beta_j^- z + i\beta_k^- z} \right) \langle \Phi_j^-, \Phi_k^- \rangle + \\
&\quad + \left(-i\bar{c}_j a_k \beta_k^- e^{-i\beta_j^- z - i\beta_k^- z} + i\bar{c}_j c_k \beta_k^- e^{-i\beta_j^- z + i\beta_k^- z} \right) \langle \Phi_j^-, \Phi_k^- \rangle \\
&= \sum_{k=1}^{2N} \left(-i|a_k|^2 \beta_k^- e^{i\beta_k^- z - i\beta_k^- z} + i\bar{a}_k c_k \beta_k^- e^{i\beta_k^- z + i\beta_k^- z} \right) + \\
&\quad + \sum_{k=1}^{2N} \left(-i\bar{c}_k a_k \beta_k^- e^{-i\beta_k^- z - i\beta_k^- z} + i|c_k|^2 \beta_k^- e^{-i\beta_k^- z + i\beta_k^- z} \right) \tag{2.6.4}
\end{aligned}$$

where the orthonormality condition defined by (2.3.6) is used. Recalling that $c_k = 0$ for all $\lambda_k^- \leq q_\infty$, then following (2.6.4), we arrive at the following constant quantity to the left of the interface:

$$-\frac{i}{\mu_0 \omega_0} (P^- - \bar{P}^-) = \frac{2}{\mu_0 \omega_0} \underbrace{\sum_{k=1}^{2N}}_{\lambda_k^- > 0} \beta_k^- (|c_k|^2 - |a_k|^2) = \mathbf{I}_{in} - \mathbf{I}_{ref} = C^- \tag{2.6.5}$$

where C^- is a constant in z and the incident and reflected wave intensities are defined by:

$$\mathbf{I}_{in} = \frac{2}{\mu_0 \omega_0} \underbrace{\sum_{k=1}^{2N}}_{\lambda_k^- > 0} \beta_k^- |c_k|^2 \quad \text{and} \quad \mathbf{I}_{ref} = \frac{2}{\mu_0 \omega_0} \underbrace{\sum_{k=1}^{2N}}_{\lambda_k^- > 0} \beta_k^- |a_k|^2 \tag{2.6.6}$$

respectively. We observe from (2.6.5) that the trapezoidal rule for the finite-difference approximation preserves conservation of $\int_{-\infty}^{\infty} (S_{0,z}) dx$ in z . From (2.6.6) we define the energy density of the reflected waves as:

$$E_k^- = \frac{2}{\mu_0 \omega_0} \beta_k^- |a_k|^2. \tag{2.6.7}$$

From (2.6.2) to the right of the interface, we compute the inner product P^+ as follows:

$$\begin{aligned}
P^+ &= \sum_{j=1}^{2N} \sum_{k=1}^{2N} \left\langle \bar{b}_j e^{-i\beta_j^+ z} \Phi_j^+, i b_k \beta_k^+ e^{i\beta_k^+ z} \Phi_k^+ \right\rangle \\
&= \sum_{j=1}^{2N} \sum_{k=1}^{2N} \left(i \bar{b}_j b_k \beta_k^+ e^{-i\beta_j^+ z + i\beta_k^+ z} \right) \langle \Phi_j^-, \Phi_k^- \rangle \\
&= \sum_{k=1}^{2N} i |b_k|^2 \beta_k^+ e^{-i\beta_j^+ z + i\beta_k^+ z} \tag{2.6.8}
\end{aligned}$$

where the same orthonormality condition (2.3.6) is used. Using (2.6.2) we find the constant quantity to the right of the interface:

$$-\frac{i}{\mu_0 \omega_0} (P^+ - \bar{P}^+) = \frac{2}{\mu_0 \omega_0} \underbrace{\sum_{k=1}^{2N} \beta_k^+ |b_k|^2}_{\lambda_k^+ > 0} = \mathbf{I}_{trans} = C^+ \tag{2.6.9}$$

where C^+ a constant in z and \mathbf{I}_{trans} is the transmitted wave intensity. From (2.6.9) we define the energy density of the transmitted waves as:

$$E_k^+ = \frac{2}{\mu_0 \omega_0} \beta_k^+ |b_k|^2. \tag{2.6.10}$$

We prove numerically that $C^- = C^+$, such that the conservation law across the interface holds:

$$\mathbf{I}_{in} = \mathbf{I}_{ref} + \mathbf{I}_{trans}. \tag{2.6.11}$$

By further normalizing the reflected and transmitted wave intensities as,

$$R = \frac{\mathbf{I}_{ref}}{\mathbf{I}_{in}} \quad \text{and} \quad T = \frac{\mathbf{I}_{trans}}{\mathbf{I}_{in}} \tag{2.6.12}$$

we rewrite (2.6.11) in the form

$$1 = R + T. \tag{2.6.13}$$

Here R is referred to as the reflectance and T is referred to as the transmittance.

2.7 Visualization of Particular Solutions

Here we verify our numerical results by simulating different waveguide configurations. For each simulation, we construct the eigenvalue spectrum as well as three-dimensional plots of the electric and magnetic field distributions in each waveguide. We also confirm conservation of energy, given by (2.6.13). The numerical results use the following list of parameters in Table 2-1.

Symbol	Definition
ρ^-	width of W^-
ρ^+	width of W^+
q_0^-	refractive index of W^-
q_0^+	refractive index of W^+
R	reflectance
T	transmittance

Table 2-1. The first four variables are the varying input parameters while the last two variables are specific output values. Notations W^- and W^+ represent the waveguide to the left and right of the interface respectively.

We use a uniform grid for the domain

$$D = D^- \cup D^+ = \{(x, z) : -\alpha_x \leq x \leq \alpha_x, -\alpha_z \leq z \leq \alpha_z\},$$

with a mesh size h (chosen independently for each simulation) for both the x and z axes. To understand our algorithm and numerical results, we compute the wave transmission for two different waveguide configurations: for varying $\frac{\rho^+}{\rho^-}$ and fixed $\frac{q_0^+}{q_0^-}$ and for fixed $\frac{\rho^+}{\rho^-}$ and varying $\frac{q_0^+}{q_0^-}$. In each case, we assume that the refractive index of air, outside each waveguide is 1, i.e. $q_\infty^\pm = 1$.

2.7.1 Varying ρ^+ , fixed q_0^+

Here we assume that both waveguides, W^- and W^+ , are engineered from identical materials and hence, have exactly the same refractive index; $q_0^+ = q_0^- = 2$. Using the domain D with $\alpha_x = \alpha_z = 30$ we construct a two-dimensional grid with mesh size $h = \frac{3}{20}$. We study how the reflectance and transmittance change with varying width ρ^+ of waveguide W^+ with respect to the width ρ^- of waveguide W^- . The latter is kept constant at $\rho^- = 1$. The results of several computations are shown in Table 2-2.

R	0.0000	0.0023	0.0050	0.0050	0.0034	0.0034	0.0033	0.0034	0.0034
T	1.0000	0.9977	0.9950	0.9950	0.9966	0.9966	0.9967	0.9967	0.9967
ρ^+	1	2	3	4	5	6	7	8	9

Table 2-2. Reflectance R and Transmittance T versus ρ^+ , for fixed $\rho^- = 1$ and $q_0^- = q_0^+ = 2$.

The reflectance R remains small compared to transmittance T . Therefore transmitted modes to the right of the interface have a significantly higher energy density (as it is defined by the *Poynting* vector) than the reflected modes to the left of the interface. As $\rho^+ \rightarrow \infty$, R approaches asymptotically to a constant value $R_\infty = 0.0034$, while T approaches to a constant value $T_\infty = 0.9967$. However, the balance equation (2.6.13) is satisfied in each computation. The graphs of T and R are shown in Figure 2-1(a) and 2-1(b).

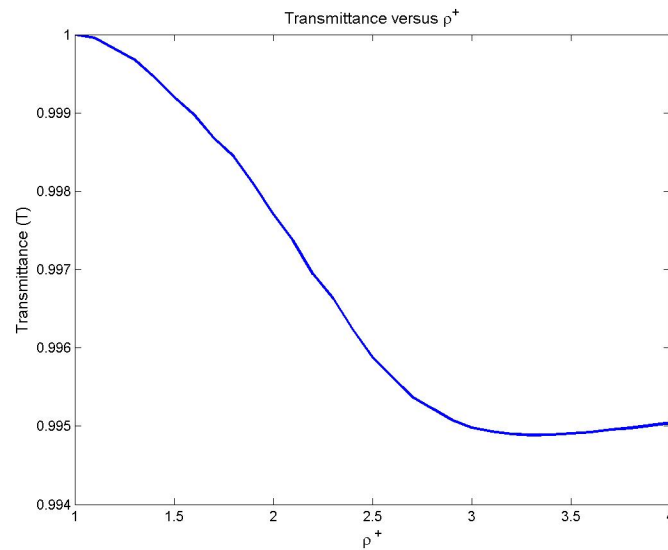


Figure 2-1(a). Transmittance T versus the width ρ^+ of the waveguide W^+ . At each value of ρ^+ , $T = 1 - R$.

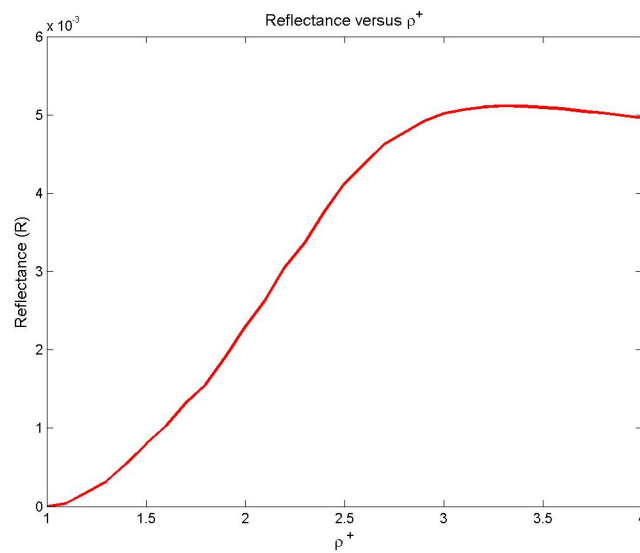


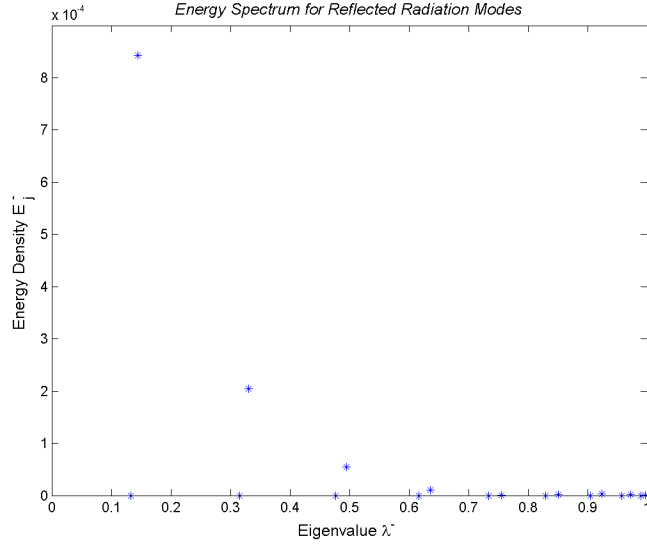
Figure 2-1(b). Reflectance R versus the width ρ^+ of the waveguide W^+ . At each value of ρ^+ , $R = 1 - T$.

Next we fix specific parameters from Table 2-2: $q_0^- = q_0^+ = 2$, $\rho^- = 1$ and $\rho^+ = 2$; i.e. we consider the interface between two planar waveguides with quantum potential

functions

$$q^-(x) = \begin{cases} 1, & \text{for } |x| \geq 1 \\ 2, & \text{for } |x| < 1 \end{cases}, \quad q^+(x) = \begin{cases} 1, & \text{for } |x| \geq 2 \\ 2, & \text{for } |x| < 2 \end{cases}, \quad (2.7.1)$$

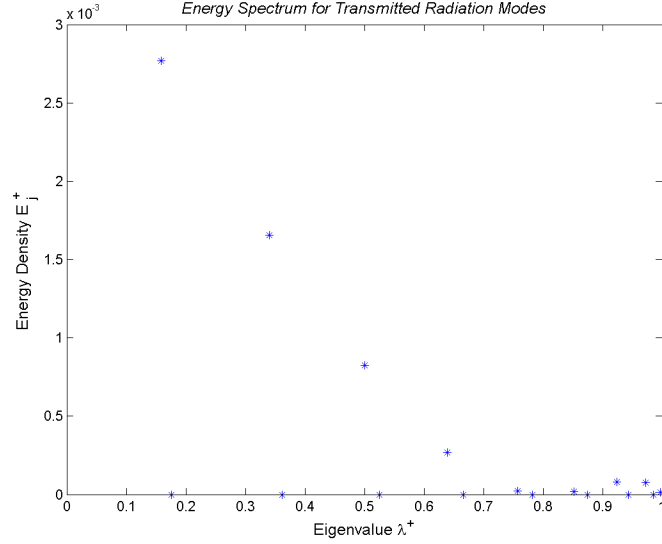
to the left and right of the interface. Using Figure 1-2, we can predict the spectrum of eigenvalues λ^- and λ^+ . Since we are only concerned in radiation modes of the continuous spectrum, $0 \leq \lambda^\pm \leq q_\infty^\pm$, and waveguide modes of the discrete spectrum, $q_\infty^\pm < \lambda^\pm < q_0^\pm$, we remove the edge modes of the continuous spectrum, $\lambda^\pm < 0$, from the remaining figures. The energy density of the radiation and waveguide modes is defined by (2.6.7) and (2.6.10). The energy spectrum is shown in Figure 2-2(a) and 2-2(b).



2-2(a). Energy spectrum for reflected radiation modes. The discrete spectrum consists of only one waveguide mode $\lambda_1^- = 1.4437$ with $E_1^- = 0.0049$.

From Figure 2-2(a) and 2-2(b), we see that our numerical computations confirm analytic predictions. Indeed, the radiation modes of the continuous spectrum are located in the intervals $0 \leq \lambda^- \leq 1$ and $0 \leq \lambda^+ \leq 1$. The waveguide modes of the

discrete spectrum are located in the intervals $1 < \lambda^- < 2$ and $1 < \lambda^+ < 2$. We also examine the relationship between reflectance, transmittance and energy density of the largest excited waveguide modes to the left and right of the interface.



2-2(b). Energy spectrum of transmitted radiation modes. The discrete spectrum consists of two waveguides modes $\lambda_1^+ = 1.7395$ and $\lambda_2^+ = 1.1115$ with the energy density $E_1^+ = 2.3913$ and $E_2^+ = 0$ respectively.

Due to the small reflectance, $R_\infty = 0.0034$, the largest excited waveguide mode to the left of the interface, $\lambda_1^- = 1.4437$, has a relatively small density, $E_1^- = 0.0049$. This opposes the largest excited waveguide mode to the right of the interface, $\lambda_1^+ = 1.7395$, which has the large energy density, $E_1^+ = 2.3913$, since transmittance, $T_\infty = 0.9967$, is much larger. We also mention that the energy density of reflected radiation modes, seen in Figure 2-2(a), is much smaller $O(10^{-4})$, compared to that of transmitted radiation modes, seen in Figure 2-2(b).

We also construct three-dimensional plots of this simulation for $\Psi^-(x, z)$ and $\Psi^+(x, z)$ in equations (2.4.1) and (2.4.2). By combining Ψ^- and Ψ^+ on the two-dimensional grid of the domains D^- and D^+ in the (x, z) -plane, we present three-dimensional plots seen on Figure 2-3(a) and 2-3(b).

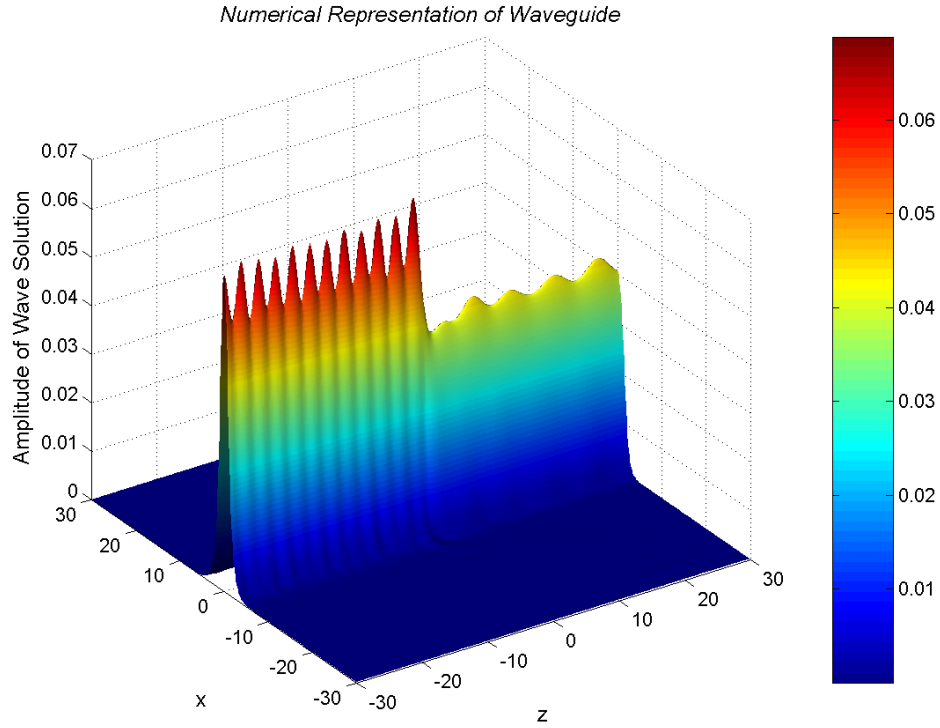


Figure 2-3(a). Visualization of the interface between two planar waveguides with parameters: $q_0^- = q_0^+ = 2$, $\rho^- = 1$ and $\rho^+ = 2$.

From Figure 2-3(a), we observe that the electromagnetic wave becomes a standing wave to the left of the interface due to reflection from the interface; in spite of the fact that reflectance R is small. Right of the interface, the periodic structure of the electromagnetic wave is due to the superposition of transmitted waveguide mode $\lambda_1^+ = 1.7395$ and radiation modes at $0 \leq \lambda^+ \leq 1$. Due to the interface configuration

radiating waves from artificial boundary-reflected waveguides are observed but are minimal, seen in Figure 2-3(b).

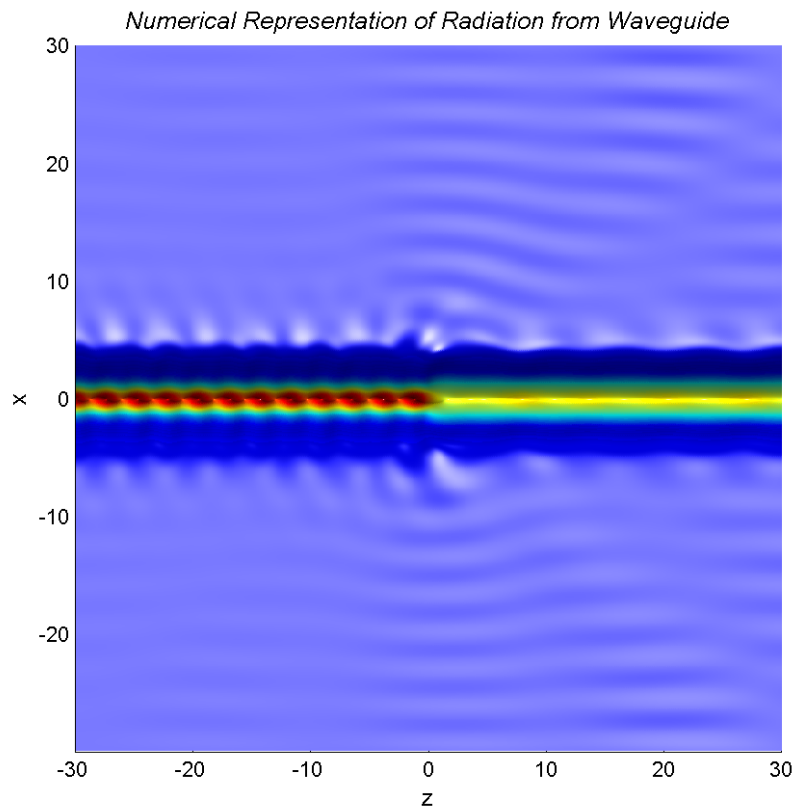


Figure 2-3(b). An elevated viewpoint of radiating waves at the interface between two planar waveguides with parameters: $q_0^- = q_0^+ = 2$, $\rho^- = 1$ and $\rho^+ = 2$.

2.7.2 Varying q_0^+ , fixed ρ^+

In this section, we assume that the two planar waveguides, W^- and W^+ are engineered from different materials and, therefore, the refractive index of each waveguide will not remain constant, as in the previous section. The geometric configuration of the interface problem is defined by the domain D with $\alpha_x = \alpha_z = 30$. The remaining parameters are defined by $h = \frac{3}{10}$, $\rho^- = 1$ and $\rho^+ = 2$. We study how the reflectance

and transmittance change with varying refractive index q_0^+ of waveguide W^+ with respect to the refractive index q_0^- of waveguide W^- . The latter is kept constant at $q_0^- = 2$. The results of several computations are shown in Table 2-3.

R	0.0018	0.0213	0.0484	0.0754	0.1005	0.1232	0.1437	0.1618	0.1771
T	0.9982	0.9787	0.9516	0.9246	0.8995	0.8768	0.8563	0.8382	0.8229
q_0^+	2	3	4	5	6	7	8	9	10

Table 2-3. Reflectance R and Transmittance T versus q_0^+ , for fixed $q_0^- = 2$, $\rho^- = 1$ and $\rho^+ = 2$.

From Table 2-3 and Figure 2-4, we see that the reflectance remains generally small, as opposed to the transmittance, but is significantly larger than the case of $q_0^- = q_0^+$. The reflectance increases, and hence, the transmittance decreases with larger ratios $\frac{q_0^+}{q_0^-}$. Still the transmitted modes to the right of the interface have a higher energy density than the reflected modes to the left of the interface. The balance equation (2.6.13) is still preserved at each computation.

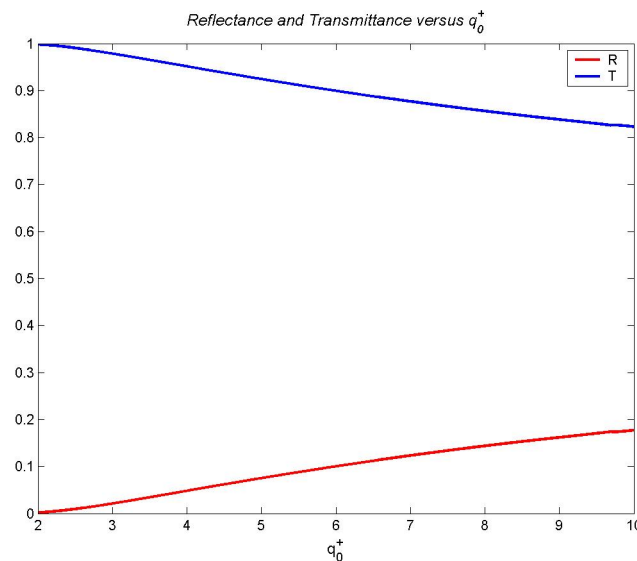


Figure 2-4. Reflectance R and transmittance T versus the refractive index q_0^+ of the waveguide W^+ . At each value of q_0^+ $1 = R + T$.

Again, we now fix specific parameters from Table 2-3: $\rho^- = 1$, $\rho^+ = 2$, $q_0^- = 1$ and $q_0^+ = 4$; i.e. we consider the interface between two planar waveguides with quantum potential functions

$$q^-(x) = \begin{cases} 1, & \text{for } |x| \geq 1 \\ 2, & \text{for } |x| < 1 \end{cases}, \quad q^+(x) = \begin{cases} 1, & \text{for } |x| \geq 2 \\ 4, & \text{for } |x| < 2 \end{cases}, \quad (2.7.2)$$

to the left and right of the interface. Using Figure 1-2, we can predict the spectrum of eigenvalues λ^- and λ^+ . Once again, we are only concerned in radiation modes of the continuous spectrum, $0 \leq \lambda^\pm \leq q_\infty^\pm$, and waveguide modes of the discrete spectrum, $q_\infty^\pm < \lambda^\pm < q_0^\pm$. Therefore we remove the edge modes of the continuous spectrum, $\lambda^\pm < 0$, from the remaining figures. The energy spectrum is shown on Figure 2-5(a) and 2-5(b).

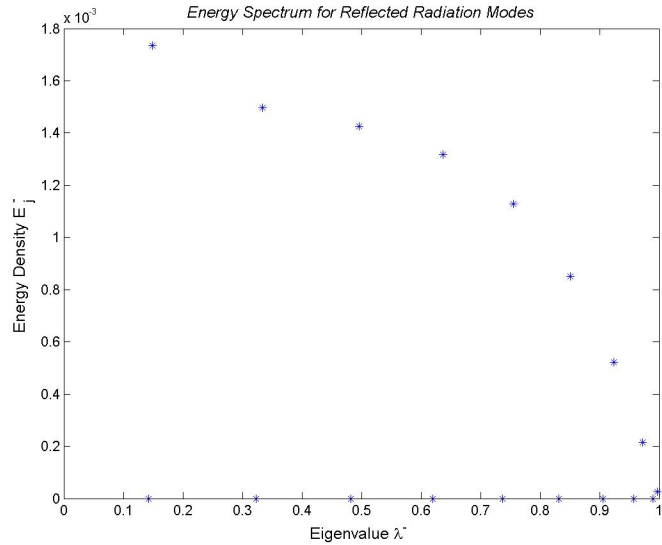


Figure 2-5(a). Energy spectrum for reflected radiation modes. The discrete spectrum consists of only one waveguide mode: $\lambda_1^- = 1.4794$ with $E_1^- = 0.1091$.

Comparing Table 2-3 with Table 2-2, we observe that the transmittance remains consistently higher than the reflectance in Table 2-3, but is lower than in Table 2-2.

Indeed, the largest excited waveguide mode to the right of the interface, $\lambda_1^+ = 3.6238$, does in fact have a significantly higher density, $E_1^+ = 2.2698$ than the corresponding waveguide mode to the left of the interface, $\lambda_1^- = 1.4794$ with $E_1^- = 0.1091$. However, we observe that E_1^+ is smaller, while E_1^- is larger than in the case of $q_0^+ = q_0^-$.

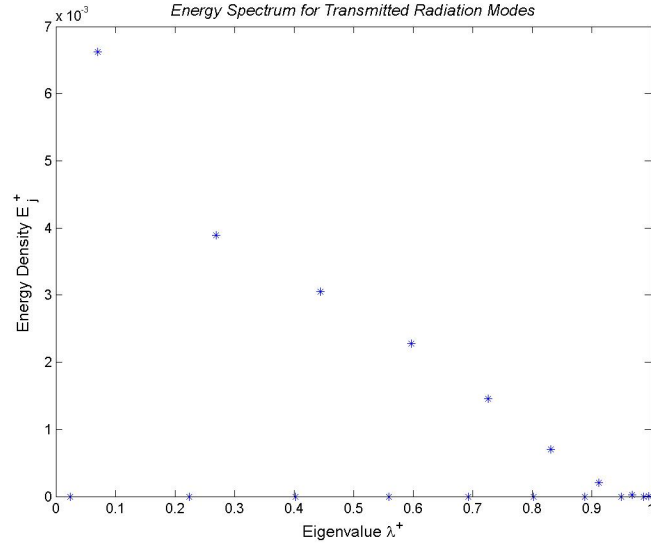


Figure 2-5(b). Energy spectrum for transmitted radiation modes. The discrete spectrum consists of three waveguide modes: $\lambda_1^+ = 3.6238$, $\lambda_2^+ = 2.5544$ and $\lambda_3^+ = 1.1270$ with the corresponding energy densities: $E_1^+ = 2.2698$, $E_2^+ = 0$ and $E_3^+ = 0.0268$.

We conclude that varying the ratio $\frac{q_0^+}{q_0^-}$ and fixing the ratio $\frac{\rho^+}{\rho^-}$ has a much larger effect on reflectance and transmittance than varying the ratio $\frac{\rho^+}{\rho^-}$ and fixing the ratio $\frac{q_0^+}{q_0^-}$. That is, by increasing the refractive index q_0^+ of the waveguide W^+ results in a significant increase of the reflectance and a decrease of the transmittance. Hence, in the infinite limit, the two curves seen in Figure 2-4 will approach one another.

We again construct three-dimensional plots of this simulation for $\Psi^-(x, z)$ and $\Psi^+(x, z)$ in equations (2.4.1) and (2.4.2). By combining Ψ^- and Ψ^+ on the two-dimensional grid of the domains D^- and D^+ in the (x, z) -plane, we present three-dimensional plots shown in Figure 2-6(a) and 2-6(b).

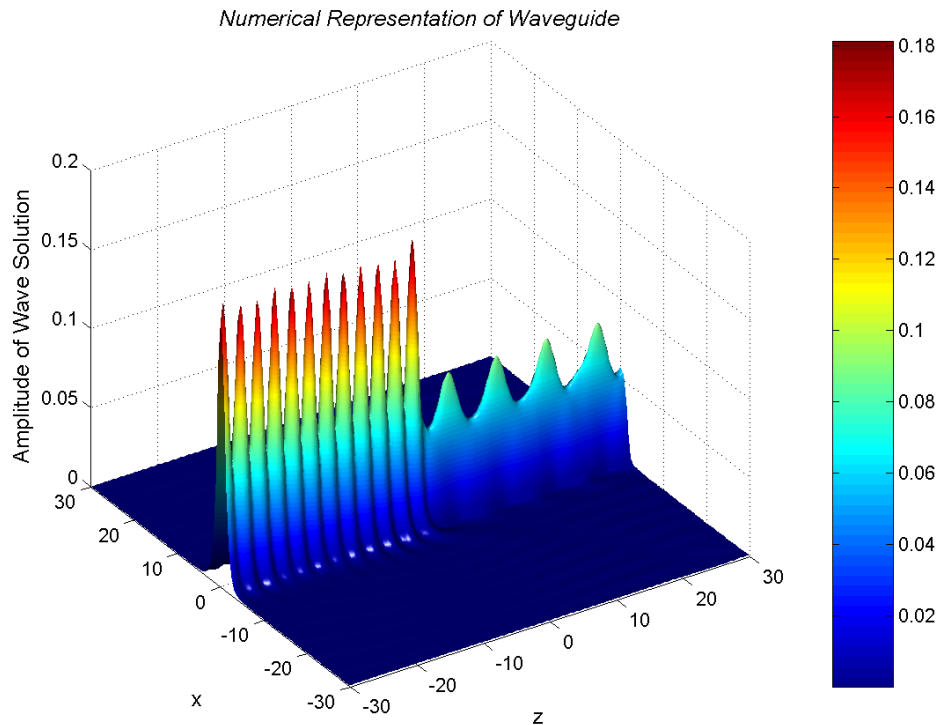


Figure 2-6(a). Visualization of the interface between two planar waveguides with parameters: $\rho^- = 1$, $\rho^+ = 2$, $q_0^- = 2$ and $q_0^+ = 4$.

From Figure 2-6(a), we observe that the electromagnetic wave becomes a standing wave to the left of the interface due to reflection from the interface; in spite of the fact that reflectance R remains small. Right of the interface, the periodic structure of the electromagnetic wave is due to the superposition of transmitted waveguide modes; $\lambda_1^+ = 3.6283$ and $\lambda_3^+ = 1.1270$ as well as radiation modes at $0 \leq \lambda^+ \leq 1$. We see

from Figure 2.6(b), the increased presence of radiating waves from artificial boundary-reflected waveguides and that radiation, due to this waveguide configuration, is much stronger than in the previous configuration. In comparing with Figure 2.3(b), we conclude; the higher the refractive index of the waveguide W^+ the larger the amount of radiation present.

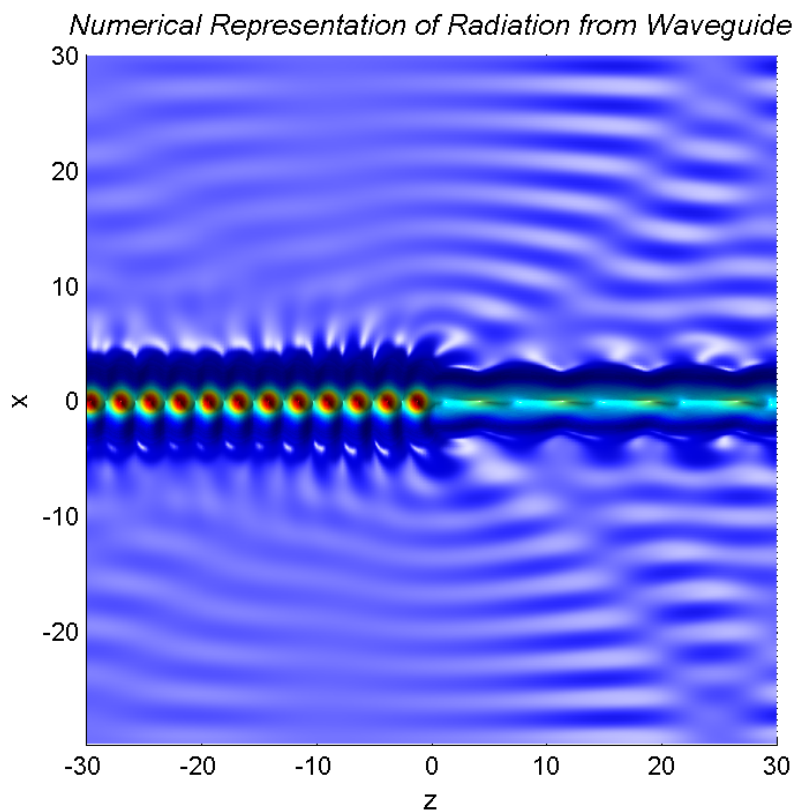


Figure 2-6(b). An elevating viewpoint of radiating waves at the interface between two planar waveguides with parameters: $\rho^- = 1$, $\rho^+ = 2$, $q_0^- = 2$ and $q_0^+ = 4$.

Chapter 3

Numerical Algorithm with Absorbing Layers

3.1 Introduction

In this chapter we modify the FDFD method with an absorbing layer, which absorbs outgoing waves from artificial boundary-reflected waveguides. By using a complexification of transverse space, we introduce a thin absorbing layer on the boundaries of the computational domain. We will once again apply the FDFD method to solve the spectral problem (1.4.4) for the one-dimensional *Schrodinger* operator on the complex plane $x \in \mathbb{C}$. The spectral problem (1.4.4) has complex eigenvalues λ and we intend to show that the complexification of transverse space results in a spectral deformation such that $\text{Im}(\lambda) \geq 0$ for eigenvalues λ of the continuous spectrum. We develop a numerical algorithm similar to that of chapter 2. The new algorithm does not rely on orthogonal spectral decompositions and projection operators. By simultaneously solving a set of algebraic equations at the interface between two planar waveguides, we construct the numerical solution which displays a full picture of electric and magnetic field distributions in each waveguide.

3.2 Complexification of Transverse Space

Here we intend to solve the eigenvalue problem (1.4.4) for the operator \mathcal{L} with an absorbing layer outside the waveguide. We introduce the absorbing layer by using the following method [3][5][15][20][27]. We consider complex values of the transverse space coordinate x . The complexification of the space variable results in the transformation of the operator \mathcal{L} into the complex operator, denoted by $\tilde{\mathcal{L}}$.

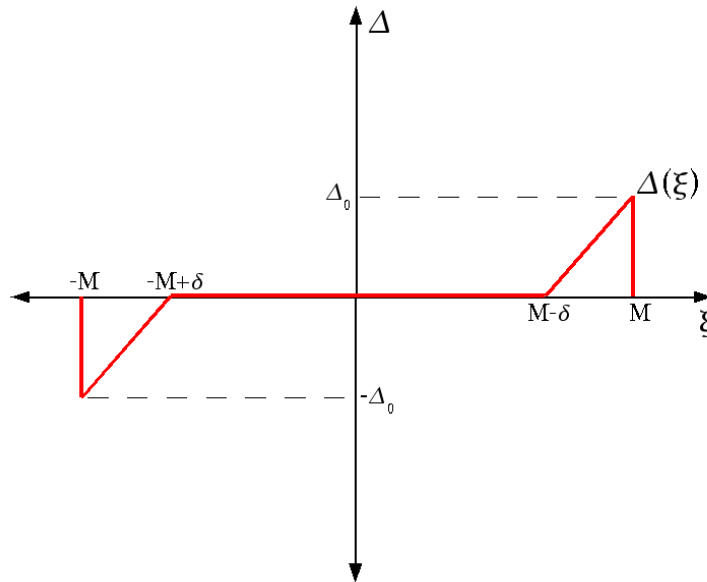


Figure 3-1. Piecewise linear absorbing function $\Delta(\xi)$.

Let x to be complex-valued such that $\text{Re}(x) = \xi$, $\xi \in \mathbb{R}$ and $\text{Im}(x) = \Delta(\xi)$, where $\Delta(\xi)$ is shown graphically in Figure 3-1. Here M is the half-width of the finite interval of the computational domain, δ is the width of the absorbing layer surrounding the computational domain, and Δ_0 is known as the damping, or absorption coefficient

[8][10] [19]. The function $\Delta(\xi)$ is given analytically by

$$\Delta(\xi) = \begin{cases} \Delta_0 \frac{\xi - M + \delta}{\delta}, & \text{for } M - \delta < \xi < M \\ 0, & \text{for } -M + \delta < \xi < M - \delta \\ \Delta_0 \frac{\xi + M - \delta}{\delta}, & \text{for } -M < \xi < -M + \delta. \end{cases} \quad (3.2.1)$$

The complexification method is applied to the linear eigenvalue problem (1.4.4),

$$\left[\frac{d^2}{dx^2} + q(x) \right] \Phi(x) = \lambda \Phi(x), \quad x = \xi + i\Delta(\xi). \quad (3.2.2)$$

We recall that the problem (3.2.2) is treated separately to the left and right of the interface. We shall show that the function $\Delta(\xi)$ with $\Delta_0 > 0$ introduces damping, or absorbing properties in the eigenvalue problem (3.2.2). Let us consider here the eigenvalue problem (3.2.2) with Dirichlet boundary conditions:

$$\Phi(\xi = \pm M) = 0. \quad (3.2.3)$$

Let us first consider the case $\xi > 0$. We recall that $q(\xi) = q_\infty \equiv \text{const}$ for $\xi > \rho$, where we assume that $\rho < M - \delta$. Let us now consider the function $\Delta(\xi) = \Delta_0 \frac{\xi - M + \delta}{\delta}$ for $\xi > M - \delta$. Then we can solve the problem (3.2.2) analytically with the general solution:

$$\Phi(x) = c_+ e^{ikx} + c_- e^{-ikx} \quad (3.2.4)$$

where $k = \sqrt{q_\infty - \lambda}$ and $\text{Re}(\lambda) < q_\infty$. Using $x = \xi + \Delta(\xi)$, the general solution (3.2.4) becomes:

$$\Phi(\xi) = c_+ e^{ik\xi} e^{-k \frac{\Delta_0}{\delta} (\xi - M + \delta)} + c_- e^{-ik\xi} e^{k \frac{\Delta_0}{\delta} (\xi - M + \delta)} \quad (3.2.5)$$

and from the Dirichlet boundary conditions at $\xi = M$, $\Phi(M) = 0$, we conclude

$$c_+ e^{ikM - k\Delta_0} = -c_- e^{-ikM + k\Delta_0}. \quad (3.2.6)$$

Therefore, the amplitudes c_+ and c_- are related as follows:

$$\frac{c_-}{c_+} = -e^{2ikM-2k\Delta_0}. \quad (3.2.7)$$

It is clear from (1.4.13) that c_+ represents the amplitude of the outgoing wave from the waveguide at $\xi = 0$ and c_- is the amplitude of the incoming wave from artificial boundary-reflected waveguides at $\xi = 2M$. From (3.2.7) we conclude that $|c_-| = |c_+|e^{-2k\Delta_0}$ decreases exponentially with larger Δ_0 for $\Delta_0 > 0$. Therefore, the complexification with $\Delta(\xi)$ for $\xi > 0$ introduces an effective damping for amplitudes of the wave from artificial boundary-reflected waveguides. A similar argument for $\xi < 0$ shows that the damping of waves from artificial boundary-reflected waveguides occur for $\Delta(\xi) < 0$.

For computational efficiency, we use a piecewise continuous linear absorption function, $\Delta(\xi)$, given by (3.2.1) [4][20][27]. To prepare for a computational solution, we rewrite (3.2.2) in terms of $\xi \in \mathbb{R}$. By using the following equations

$$\frac{d\Phi}{d\xi} = \frac{d\Phi}{dx} \left(1 + i \frac{d\Delta}{d\xi} \right) \quad (3.2.8)$$

and

$$\frac{d^2\Phi}{d\xi^2} = \left[\frac{d^2\Phi}{dx^2} \left(1 + i \frac{d\Delta}{d\xi} \right) + \frac{d\Phi}{dx} i \frac{d^2\Delta}{d\xi^2} \right] \left(1 + i \frac{d\Delta}{d\xi} \right) \quad (3.2.9)$$

(3.2.2) becomes

$$\left[\frac{1}{C(\xi)} \frac{d^2}{d\xi^2} + q(\xi) \right] \Phi(\xi) = \lambda \Phi(\xi), \quad \lambda \in \mathbb{C}, \xi \in \mathbb{R} \quad (3.2.10)$$

where

$$C(\xi) = 1 + i \frac{d\Delta}{d\xi} = \begin{cases} 1, & \text{for } -M + \delta < \xi < M - \delta \\ 1 + i \frac{\Delta_0}{\delta}, & \text{otherwise.} \end{cases} \quad (3.2.11)$$

Thus, the eigenvalue problem $\mathcal{L}\Phi(x) = \lambda\Phi(x)$ is equivalent to the eigenvalue problem $\tilde{\mathcal{L}}\Phi(\xi) = \lambda\Phi(\xi)$ where $\tilde{\mathcal{L}}$ is defined by

$$\tilde{\mathcal{L}} = \frac{1}{C(\xi)} \frac{d^2}{d\xi^2} + q(\xi). \quad (3.2.12)$$

In the next section, we apply the FDFD method to construct the eigenvalue spectrum of the transformed operator $\tilde{\mathcal{L}}$. When $q(\xi)$ is a compact potential, such that $q(\xi) = q_\infty$ for $|\xi| > \rho$, it follows from (3.2.10) that the continuous spectrum is located for

$$\tilde{\mathcal{L}}_C = \{\lambda \in \mathbb{C} : \text{Re}(\lambda) < q_\infty\}. \quad (3.2.13)$$

The absorbing layer does not essentially change the location and number of eigenvalues of discrete spectrum, since the eigenfunctions $\Phi(\xi)$ are exponentially small at the absorbing layer $|\xi| > M - \delta$. This fact will be verified numerically in section 3.5.

Recall from chapter 1 that $\mathcal{L}_C = \{\lambda \in \mathbb{R} : \lambda \leq q_\infty\}$. By introducing an absorbing layer around the computation domain, we show that the complexification of transverse space results in a spectral deformation of \mathcal{L}_C to $\tilde{\mathcal{L}}_C$ such that $\text{Im}(\lambda) \geq 0$ for $\lambda \in \tilde{\mathcal{L}}_C$. Also we show that the initial effect of the spectral deformation is a clockwise rotation of the continuous spectrum \mathcal{L}_C about q_∞ through an angle θ . The result of this rotation is the deformed spectrum $\tilde{\mathcal{L}}_C$.

Let us consider here the eigenvalue problem (3.2.10) with Dirichlet boundary conditions (3.2.3). We simplify the consideration by removing the waveguide configuration, i.e. $q(\xi) = q_\infty \equiv \text{const}$ for $-M < \xi < M$, and filling the absorbing function in the entire computational domain, i.e. $C(\xi) = 1 + i\frac{\Delta_0}{M} = C_0 \equiv \text{const}$. Then we can solve the problem (3.2.10) analytically with the general solution:

$$\Phi(\xi) = a_+ e^{i\gamma\xi} + a_- e^{-i\gamma\xi} \quad (3.2.14)$$

where $-\frac{\gamma^2}{C_0} + q_\infty = \lambda$ implying that

$$\lambda = q_\infty - \frac{\gamma^2(1 - \frac{i\Delta_0}{\delta})}{1 + \frac{\Delta_0^2}{\delta^2}}. \quad (3.2.15)$$

Following (3.2.15) we define the real and imaginary parts of the eigenvalue λ as:

$$\operatorname{Re}(\lambda) = q_\infty - \frac{\gamma^2\delta^2}{\delta^2 + \Delta_0^2} \quad (3.2.16)$$

and

$$\operatorname{Im}(\lambda) = \frac{\gamma^2\Delta_0\delta}{\delta^2 + \Delta_0^2} \quad (3.2.17)$$

where γ parameterizes λ . From the Dirichlet boundary conditions at $\xi = \pm M$, $\Phi(\pm M) = 0$, we conclude that

$$2i \sin 2\gamma M = 0 \Rightarrow \gamma = \gamma_n = \frac{\pi n}{2M}, \quad n \in \mathbb{Z} \quad (3.2.18)$$

which, using (3.2.15), defines the location of the eigenvalues λ_n of the continuous spectrum $\tilde{\mathcal{L}}_C$.

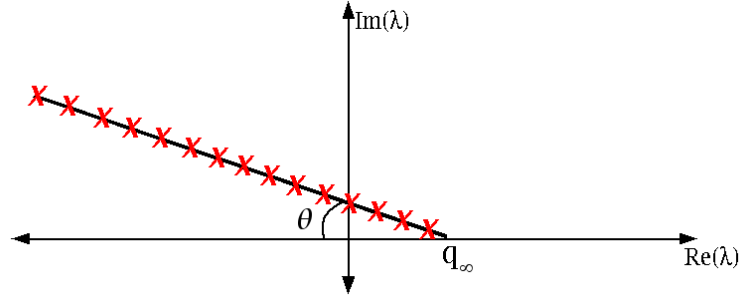


Figure 3-2. $\operatorname{Re}(\lambda)$ vs. $\operatorname{Im}(\lambda)$ for $\lambda \in \tilde{\mathcal{L}}_C$. This continuous set of eigenvalues is a rotation of \mathcal{L}_C about the point q_∞ , through an angle $\theta = -\frac{\Delta_0}{\delta}$.

Therefore, from (3.2.16) and (3.2.17) we conclude:

$$\operatorname{Im}(\lambda_n) = \frac{\Delta_0}{\delta}(q_\infty - \operatorname{Re}(\lambda_n)), \quad (3.2.19)$$

yielding a relation between the real and imaginary parts of the eigenvalues $\lambda \in \tilde{\mathcal{L}}_C$. Using the relation (3.2.19), and following the discussion on page 167 of [13], we determine that the spectrum $\tilde{\mathcal{L}}_C$ is the result of a clockwise rotation, of \mathcal{L}_C , about $q_\infty \in \mathbb{R}$, through the angle $\theta = -\frac{\Delta_0}{\delta}$; seen in Figure 3-2.

When the absorbing layer has a gap near the mid-point $\xi = 0$, splitting of the rotated continuous spectrum $\tilde{\mathcal{L}}_C$ into two distinct branches occurs. This fact will also be observed and explained numerically in section 3.5.

3.3 Finite-Difference Frequency-Domain Method

Here we search for eigenvalues of the operator $\tilde{\mathcal{L}}$, that satisfy (3.2.10) to the left and right of the interface. The eigenvalues λ are complex-valued if $C(\xi)$ is complex-valued. We consider separately, each side of the interface and work on a finite interval $-M < \xi < M$ with the FDFD method. We supplement the Dirichlet boundary conditions given by

$$\Phi(\pm M) = 0, \quad (3.3.1)$$

but extensions to other boundary conditions are similar.

As in chapter two, we solve the boundary value problem (3.2.10) with (3.3.1) by approximating the derivative terms with finite numerical differences. This generates a system of algebraic equations that can be solved. The numerical solution approximates the eigenfunction $\Phi(\xi)$ at discrete points:

$$\xi_n = -M + nh, \quad n = 0, 1, 2, \dots, (2N - 1), 2N$$

where $h = \frac{M}{N}$ is the grid size and the interval $[-M, M]$ is partitioned into $2N$ subintervals of equal length. The points $\xi_0 = -M$ and $\xi_{2N} = M$ are the boundary grid

points, while the points ξ_n for $n = 1, 2, \dots, 2N - 1$ are the interior grid points.

The second derivative $\Phi''(\xi_n)$ is approximated by the central difference formula [11]

$$\Phi''(\xi_n) \approx \frac{\Phi(\xi_{n+1}) + \Phi(\xi_{n-1}) - 2\Phi(\xi_n)}{h^2} \quad (3.3.2)$$

where the truncation error of order $O(h^2)$ is neglected. To simplify the notation, let Φ_n denote a numerical approximation of $\Phi(\xi_n)$. Then by using the finite difference approximation in (3.3.2), we get the following discrete approximation at $\xi = \xi_n$ to the second order differential equation (3.2.10):

$$\frac{\Phi_{n+1} + \Phi_{n-1}}{C_n} + \Phi_n \left(h^2 q_n - \frac{2}{C_n} \right) = \lambda h^2 \Phi_n, \quad n = 2, 3, \dots, 2N - 2 \quad (3.3.3)$$

where $q_n = q(\xi_n)$ and $C_n = C(\xi_n)$. Note that (3.3.3) is only applied at interior grid points of the integration interval. At the boundary points, we have $\Phi_0 = \Phi_{2N} = 0$. Thus, the two boundary condition equations at $n = 1$ and $n = 2N - 1$ have the form:

$$\frac{\Phi_2}{C_1} + \Phi_1 \left(h^2 q_1 - \frac{2}{C_1} \right) = \lambda h^2 \Phi_1, \quad (3.3.4)$$

and

$$\frac{\Phi_{2N-2}}{C_{2N-1}} + \Phi_{2N-1} \left(h^2 q_{2N-1} - \frac{2}{C_{2N-1}} \right) = \lambda h^2 \Phi_{2N-1}. \quad (3.3.5)$$

Taken together, equations (3.3.3)-(3.3.5), constitute a system of $2N - 1$ linear algebraic equations in the vector of $2N - 1$ unknowns $\Phi = (\Phi_1, \Phi_2, \dots, \Phi_{2N-1})^T$. Since $q(\xi)$ and $C(\xi)$ are known functions of ξ , the system above is equivalent to the linear eigenvalue system

$$A\Phi = \lambda h^2 \Phi, \quad (3.3.6)$$

where

$$A = \begin{pmatrix} Q_1 & \frac{1}{C_1} & 0 & & \dots & 0 \\ \frac{1}{C_2} & Q_2 & \frac{1}{C_2} & 0 & \dots & 0 \\ 0 & \frac{1}{C_3} & Q_3 & \frac{1}{C_3} & 0 \dots & 0 \\ \vdots & & & \ddots & & \vdots \\ 0 & & \dots & \frac{1}{C_{2N-2}} & Q_{2N-2} & \frac{1}{C_{2N-2}} \\ 0 & 0 & \dots & 0 & \frac{1}{C_{2N-1}} & Q_{2N-1} \end{pmatrix}$$

and

$$Q_n = h^2 q_n - \frac{2}{C_n}, \quad n = 1, 2, \dots, 2N - 1.$$

The coefficient matrix A is tridiagonal, and therefore, numerical solution of the linear boundary value problem (3.3.6) simplifies considerably using the LU decomposition algorithm; even for large values of N [11].

Using (3.3.6), we arrive at the following complex eigenvalue problem to the left of the interface:

$$A^- \Phi_j^- = \lambda_j^- h^2 \Phi_j^- \quad j = 1, 2, \dots, 2N - 1. \quad (3.3.7)$$

Following (3.3.7), there exists $\{\lambda_j^-\}_{j=1}^{2N-1}$ and $\{\Phi_j^-\}_{j=1}^{2N-1}$ where $\lambda_j^- \in \mathbb{C}$ is an eigenvalue of A^- with corresponding eigenvector $\Phi_j^- \in \mathbb{C}^{2N-1}$. We order eigenvalues according to their real parts into eigenvalues for edge modes $\text{Re}(\lambda_j^-) < 0$, radiation modes $0 < \text{Re}(\lambda_j^-) < q_\infty$, and waveguide modes $q_\infty < \text{Re}(\lambda_j^-) < q_0$. Again, referring to (3.3.6) we have the complex eigenvalue problem right of the interface:

$$A^+ \Phi_j^+ = \lambda_j^+ h^2 \Phi_j^+ \quad j = 1, 2, \dots, 2N - 1. \quad (3.3.8)$$

Following (3.3.8), there exists $\{\lambda_j^+\}_{j=1}^{2N-1}$ and $\{\Phi_j^+\}_{j=1}^{2N-1}$ where $\lambda_j^+ \in \mathbb{C}$ is an eigenvalue of A^+ with corresponding eigenvector $\Phi_j^+ \in \mathbb{C}^{2N-1}$. We emphasize here that the eigenvectors $\{\Phi_j^-\}_{j=1}^{2N-1}$ and $\{\Phi_j^+\}_{j=1}^{2N-1}$ are not orthogonal, since the complex-valued matrices A^\pm are not Hermitian.

3.4 Solutions of the Interface Equations

Similarly to chapter 2.4, we use the matching conditions at the interface and find a system of $2N - 1$ equations with $2N - 1$ unknowns. A solution of the interface equations yields the reflected and transmitted wave coefficients; $\{a_j\}_{j=1}^{2N-1}$ and $\{b_j\}_{j=1}^{2N-1}$. According to (1.4.14) and using (3.3.7) and (3.3.8), for $z < 0$ and $z > 0$, the FDFD method produces the identical representation for $\Psi^\pm(z)$, as in (2.4.1) and (2.4.2) respectively.

At the interface $z = 0$, we have the continuity equations given by (1.5.12) which yield a system of linear equations similar to (2.4.3)-(2.4.4) for coefficients a_j, b_j . This system is rewritten in this setting as:

$$\sum_{j=1}^{2N-1} c_j \Phi_j^- + \sum_{j=1}^{2N-1} a_j \Phi_j^- = \sum_{j=1}^{2N-1} b_j \Phi_j^+ \quad (3.4.1)$$

$$\sum_{j=1}^{2N-1} \beta_j^- c_j \Phi_j^- - \sum_{j=1}^{2N-1} \beta_j^- a_j \Phi_j^- = \sum_{j=1}^{2N-1} \beta_j^+ b_j \Phi_j^+. \quad (3.4.2)$$

Since the matrices A^\pm are not Hermitian, the eigenvalues λ^\pm are complex-valued. Hence, the matrices A^\pm cannot be diagonalized and the eigenvectors $\{\Phi_j^-\}_{j=1}^{2N-1}$ and $\{\Phi_j^+\}_{j=1}^{2N-1}$ do not form an orthonormal basis for \mathbb{C}^{2N-1} . Therefore, we are unable to solve the system of equations (3.4.1)-(3.4.2) using projection operators as we did in section 2.5. Without the use of projection operators constructing the set of reflected $\{a_j\}_{j=1}^{2N-1}$, and transmitted $\{b_j\}_{j=1}^{2N-1}$ wave coefficients is equivalent to finding a solution to the following linear matrix equation

$$\Lambda \Omega = \Upsilon. \quad (3.4.3)$$

The matrix Λ is a $(4N - 2)$ -by- $(4N - 2)$ block matrix defined by

$$\Lambda = \begin{pmatrix} \Lambda_1 & \Lambda_2 \\ \Lambda_3 & \Lambda_4 \end{pmatrix}$$

where each $(2N - 1)$ -by- $(2N - 1)$ block is given by

$$\Lambda_1 = -(\Phi_1^-, \Phi_2^-, \dots, \Phi_{2N-1}^-), \quad \Lambda_2 = (\Phi_1^+, \Phi_2^+, \dots, \Phi_{2N-1}^+),$$

$$\Lambda_3 = (\beta_1^- \Phi_1^-, \beta_2^- \Phi_2^-, \dots, \beta_{2N-1}^- \Phi_{2N-1}^-), \quad \Lambda_4 = (\beta_1^+ \Phi_1^+, \beta_2^+ \Phi_2^+, \dots, \beta_{2N-1}^+ \Phi_{2N-1}^+).$$

The known vector Υ is $(4N - 2)$ -dimensional and is defined by

$$\Upsilon = \sum_{j=1}^{2N-1} [c_j(\Phi_j^-, \beta_j^- \Phi_j^-)^T]. \quad (3.4.4)$$

The unknown vector Ω represents the reflected $\mathbf{a} = (a_1, a_2, \dots, a_{2N-1})^T$ and transmitted $\mathbf{b} = (b_1, b_2, \dots, b_{2N-1})^T$ coefficients:

$$\Omega = (\mathbf{a}, \mathbf{b})^T. \quad (3.4.5)$$

When Λ is non-singular, a unique solution of (3.4.3) is written in the form:

$$\Omega = \Lambda^{-1} \Upsilon. \quad (3.4.6)$$

If Λ is singular than a generic perturbation of the step size h will shift eigenvalues of Λ and result in a non-singular matrix Λ .

Together, with the vectors \mathbf{a} , \mathbf{b} and \mathbf{c} of reflected, transmitted and incident wave coefficients, with the eigenvalues to the left and right of the interface, we recover vector solutions $\Psi^-(z)$ and $\Psi^+(z)$ respectively. We combine these vector representations with the spectrum of $\tilde{\mathcal{L}}$ to construct a visualization of the transmission of the electromagnetic waves through the interface with absorbing layers.

3.5 Visualization of Particular Solutions

Here we apply our numerical algorithm to simulating different waveguide configurations. To observe the effects of the absorbing layer around the computational domain, we construct plots of the energy spectrum, the location of eigenvalues as well as three-dimensional plots of the electric and magnetic field distributions in each waveguide. The two main issues we resolve numerically are: (1) the spectral deformation of the continuous spectrum and the distribution of the discrete spectrum; and (2) the ability to effectively absorb outgoing waves from mirror-reflected waveguides, i.e. radiating waves, due to the complexification of transverse space. The numerical results use the following list of parameters in Table 3-1.

Symbol	Definition
ρ^-	width of W^-
ρ^+	width of W^+
q_0^-	refractive index of W^-
q_0^+	refractive index of W^+
δ	thickness of the absorption layer
Δ_0	Damping coefficient

Table 3-1. The variables in the above table specified user input quantities. Notations W^- and W^+ represent the waveguide to the left and right of the interface respectively.

We again use a uniform grid for the domain

$$D = D^- \cup D^+ = \{(\xi, z) : -\alpha_\xi \leq \xi \leq \alpha_\xi, -\alpha_z \leq z \leq \alpha_z\},$$

with a mesh size h for both the ξ and z axes. To understand numerical results, due to this new absorbing layer, we compute the wave transmission for three different

damping coefficients, under identical waveguide configurations. We will assume that the thickness of the absorbing layer is half the width from the z -axis to the boundary, i.e. $\delta = \frac{\alpha\xi}{2}$.

We will use values $\alpha_\xi = \alpha_z = 30$ and $h = \frac{3}{10}$. We consider the wave transmission when the waveguides W^- and W^+ are engineered from different materials and are of different widths, i.e. $\rho^- = 1$, $\rho^+ = 2$, $q_0^- = 2$ and $q_0^+ = 4$. Once again, we also assume that the refractive index of air, outside each waveguide is 1, i.e. $q_\infty^\pm = 1$. Hence, we are considering the interface between two planar waveguides with quantum potential functions

$$q^-(\xi) = \begin{cases} 1, & \text{for } |\xi| \geq 1 \\ 2, & \text{for } |\xi| < 1 \end{cases}, \quad q^+(\xi) = \begin{cases} 1, & \text{for } |\xi| \geq 2 \\ 4, & \text{for } |\xi| < 2 \end{cases}, \quad (3.5.1)$$

to the left and right of the interface respectively. These are the same quantum potential functions described in section 2.7.2 for the variable $\xi \in \mathbb{R}$. Our main difference here is the absorbing layer around the boundaries of the computational domain. We will use here the value $\Delta_0 = 0.1$ and compare our new results with numerical results of section 2.7.2.

Similarly to the energy density, E_j^- of the reflected waves, to the left of the interface, given by (2.6.7), we define the energy density here as:

$$P_k^- = \frac{2}{\mu_0\omega_0} \sqrt{|\lambda^-|} |a_k|^2 \quad (3.5.2)$$

where we ensure that $\langle \Phi_{\mathbf{k}}^-, \Phi_{\mathbf{k}}^- \rangle = 1$. However $\langle \Phi_{\mathbf{j}}^-, \Phi_{\mathbf{k}}^- \rangle \neq 0$ for $j \neq k$ generally, since A^- is a non-Hermitian matrix. To the right of the interface we define the energy density as:

$$P_k^+ = \frac{2}{\mu_0\omega_0} \sqrt{|\lambda^+|} |b_k|^2 \quad (3.5.3)$$

where again $\langle \Phi_k^+, \Phi_k^+ \rangle = 1$ and $\langle \Phi_j^+, \Phi_k^+ \rangle \neq 0$ for $j \neq k$ generally. We emphasize that the energy densities P_k^\pm do not have any physical meaning in the case of an absorbing layer, since the energy is not conserved in the system. We use P_k^\pm to measure the magnitude of waveguide, radiation and edge modes. To the left and right of the interface, we also define $\tilde{\mathcal{L}}_C^\pm$ to mean the continuous spectrum corresponding to eigenvalues λ^\pm .

We study the spectral properties of the deformed continuous spectrum $\tilde{\mathcal{L}}_C^\pm$ and the distribution of the discrete spectrum. We begin by observing the location of eigenvalues $\lambda^\pm \in \tilde{\mathcal{L}}_C^\pm$, to the left and right of the interface, plotted in Figure 3-3(a) and 3-3(b) respectively.

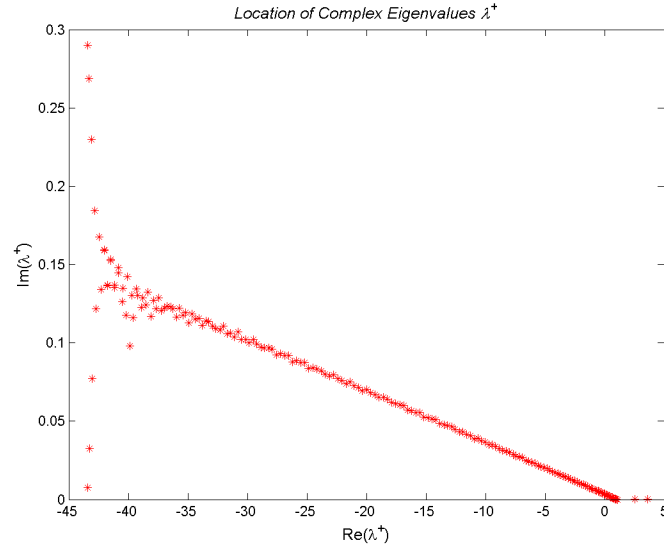


Figure 3-3(a). Location of complex eigenvalues λ^+ to the right of the interface with damping $\Delta_0 = 0.1$.

By observing figure 3-3(a), we see that all eigenvalues λ^+ that are waveguide modes of the waveguide W^+ lie on the interval $1 = q_\infty^+ < \text{Re}(\lambda^+) < q_0^+ = 4$ with $\text{Im}(\lambda^+) = 0$. Upon further investigation, the waveguide modes $\lambda_1^+ = 3.6238$, $\lambda_2^+ =$

2.5544 and $\lambda_3^+ = 1.1270$, with corresponding energy density $P_1^+ = 2.2690$, $P_2^+ = 0$ and $P_3^+ = 0.0342$, are identical to the waveguide modes λ_j^+ for $j = 1, 2, 3$, resulting from the computation of chapter 2.7.2, without the use of an absorbing layer. In fact, for no absorbing layers $\Delta_0 = 0$, the corresponding energy density $E_1^+ = 2.2691$, $E_2^+ = 0$ and $E_3^+ = 0.0346$, is essentially the same as well. The energy density for waveguide modes λ^+ with and without absorbing layers is defined by (3.5.3) and (2.6.10) respectively.

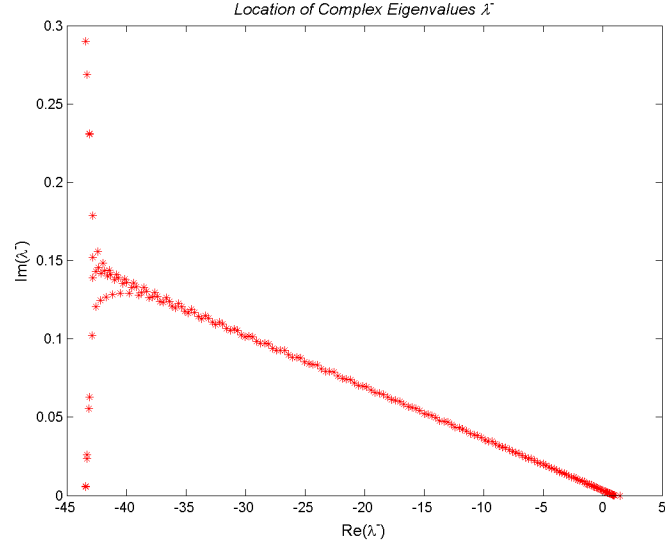


Figure 3-3(b). Location of complex eigenvalues λ^- to the left of the interface with damping $\Delta_0 = 0.1$.

From Figure 3-3(b), the only eigenvalue, corresponding to the waveguide W^- , satisfying $1 = q_\infty^- < \text{Re}(\lambda^-) < q_0^- = 2$ with $\text{Im}(\lambda^-) = 0$, is the waveguide mode $\lambda_1^- = 1.4794$ with corresponding energy density $P_1^- = 0.1088$. Again, for no absorbing layer $\Delta_0 = 0$, this is the identical waveguide mode λ_1^- with identical energy density $E_1^- = 0.1088$. The energy density for waveguide modes λ^- with and without absorbing layers is defined by (3.5.2) and (2.6.7) respectively. Therefore, we conclude that

$P_j^\pm \approx E_j^\pm$ for waveguide modes λ^\pm yielding how unaffected they are by the presence of an absorbing layer. Thus, we confirm numerically that the absorbing layer does not change the location of eigenvalues of the discrete spectrum.

Both Figure 3-3(a) and 3-3(b) reveal how the continuous spectrum $\tilde{\mathcal{L}}_C^\pm$ with absorbing layers is deformed from the continuous spectrum \mathcal{L}_C^\pm without absorbing layers. From chapter 1, we know that without absorbing layers $\Delta_0 = 0$, all eigenvalues $\lambda^\pm \in \mathcal{L}_C^\pm$ are real-valued with $\text{Im}(\lambda^\pm) = 0$. With the presence of a uniform absorbing layer, described in section 3.2, we observe that deformation of the continuous spectrum $\tilde{\mathcal{L}}_C^\pm$ is a simple clockwise rotation of \mathcal{L}_C^\pm about the point q_∞^\pm in the complex plane. We notice from Figure 3-3(a) and (b) that the absorbing layer with gap centered at $\xi = 0$ induces splitting into two distinct branches; where $\text{Im}(\lambda^\pm)$ increases on the upper branch and $\text{Im}(\lambda^\pm)$ decreases and on the lower branch. The location of the splitting boundary and the variance in splitted eigenvalues are dependent on the damping coefficient Δ_0 .

We now concern ourselves with the energy spectrum shown in Figure 3-4(a) and 3-4(b). We recall that the energy density of the radiation, edge and waveguide modes is defined by equations (3.5.2) and (3.5.3). From Figure 3-4(a) and 3-4(b), we see that our numerical results are in agreement with analytic predictions. Indeed, the continuous spectrum modes $\lambda^\pm \in \tilde{\mathcal{L}}_C^\pm$ are located in the interval where $\text{Re}(\lambda^\pm) < q_\infty^\pm$ and from previous observations we know that waveguide modes λ^\pm of the discrete spectrum are unaffected by the presence of an absorbing layer and are located where $q_\infty^\pm < \lambda^\pm < q_0^\pm$.

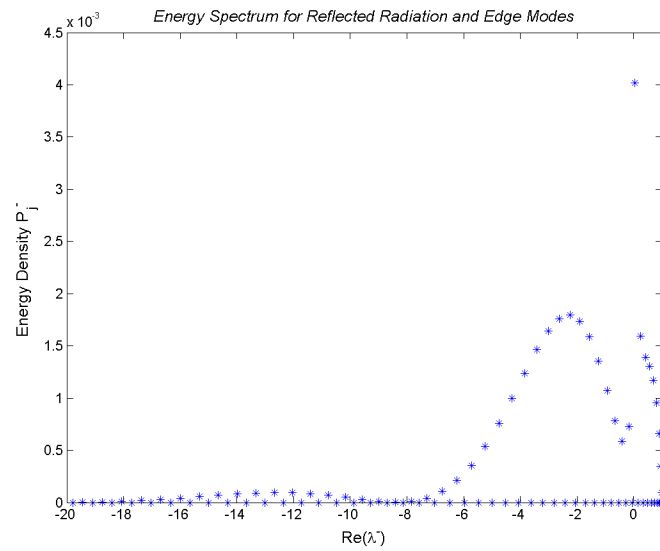


Figure 3-4(a). Energy spectrum of reflected radiation and edge modes with damping $\Delta_0 = 0.1$. The trapped waveguide mode $\lambda_1^- = 1.4794$ has corresponding energy density $P_1^- = 0.1088$.

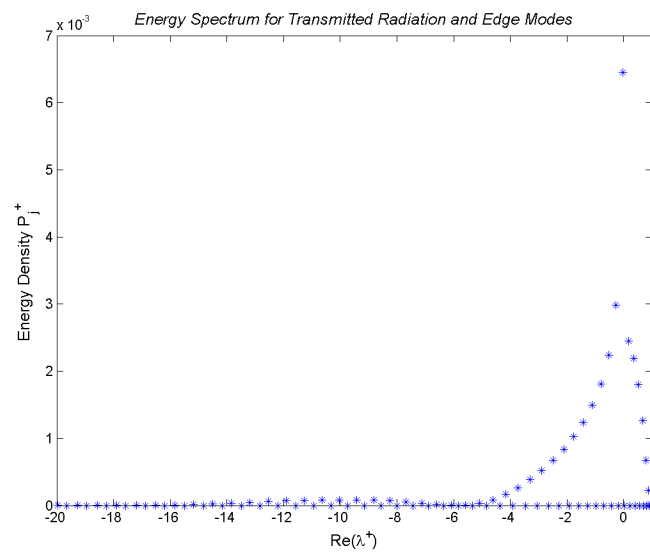


Figure 3-4(b). Energy spectrum of transmitted radiation and edge modes with damping $\Delta_0 = 0.1$. The three trapped waveguide modes: $\lambda_1^+ = 3.6238$, $\lambda_2^+ = 2.5544$ and $\lambda_3^+ = 1.1270$ have corresponding energy density: $P_1^+ = 2.2690$, $P_2^+ = 0$ and $P_3^+ = 0.0342$.

We also construct three-dimensional plots for $\Psi^-(\xi, z)$ and $\Psi^+(\xi, z)$ in equations (2.4.1) and (2.4.2). By combining Ψ^- and Ψ^+ on the two-dimensional grid of the domains D^- and D^+ in the (ξ, z) -plane, we present three-dimensional plots seen on Figure 3-5(a) and 3-5(b).

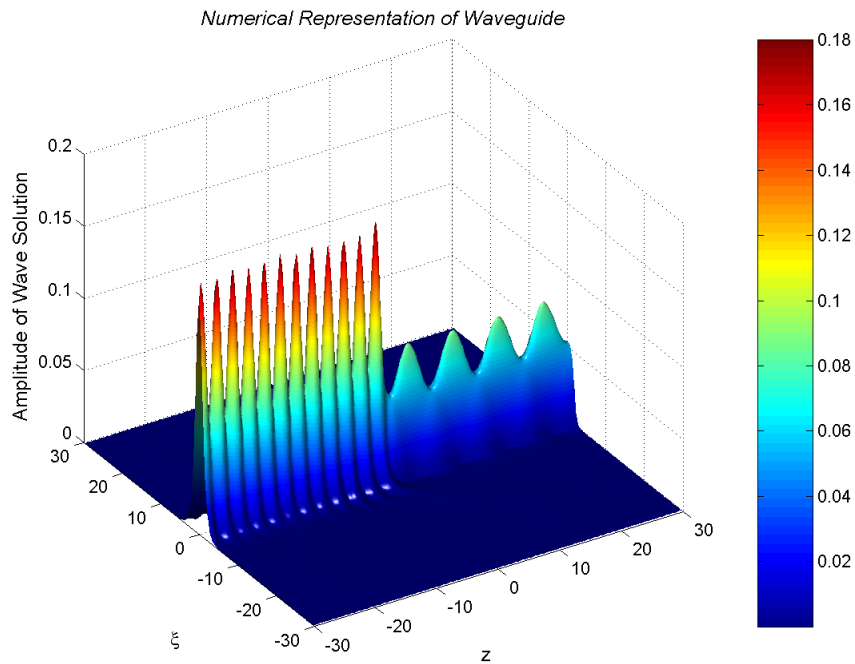


Figure 3-5(a). Visualization of the interface between two planar waveguides with parameters: $q_0^- = 2$, $q_0^+ = 4$, $\rho^- = 1$ and $\rho^+ = 2$. For the absorbing layer: $\Delta_0 = 0.1$ and $\delta = 15$.

The three-dimensional visualization of Figure 3-5(a) is very similar to Figure 2-6(a) of section 2.7.2. We again see the electromagnetic wave becomes a standing wave to the left of the interface due to the reflection from the interface. To the right of the interface the periodic structure is due to the superposition of transmitted waveguide modes; $\lambda_1^+ = 3.6283$ and $\lambda_3^+ = 1.1270$ as well as radiation modes where $0 < \text{Re}(\lambda^+) < 1$.

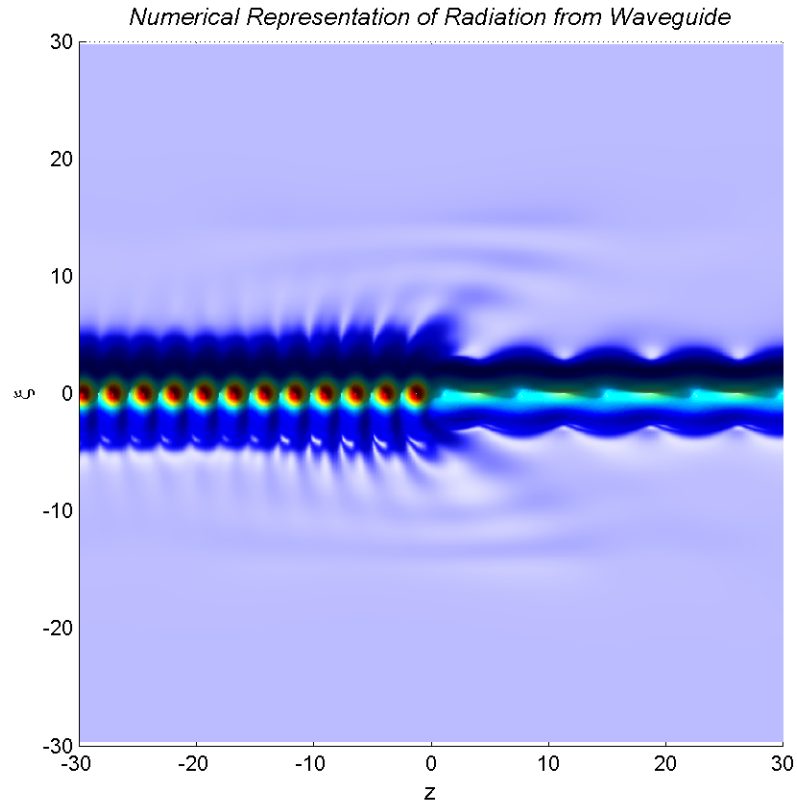


Figure 3-5(b). An elevating viewpoint of radiating waves at the interface between two planar waveguides with parameters: $q_0^- = 2$, $q_0^+ = 4$, $\rho^- = 1$ and $\rho^+ = 2$. For the absorbing layer: $\Delta_0 = 0.1$ and $\delta = 15$.

The implications of introducing an absorbing layer are not seen visually through Figure 3-5(a) but are evident in Figure 3-5(b). Due to the complexification of transverse space, we have introduced an absorbing layer that effectively absorbs radiating waves from artificial boundary-reflected waveguides. We see that all radiating waves escaping the waveguide are effectively trapped by the absorbing layer, which is located at $|\xi| > 15$. Therefore, our modified PML technique for the FDFD method produces a very efficient algorithm for reducing radiation from mirror-reflected unphysical waveguides.

3.6 The Splitting Phenomena

This section explains the splitting of eigenvalues of the continuous spectrum $\tilde{\mathcal{L}}_C$ observed in Figure 3-3(a) and (b). To show that this effect is due to the gap in the linear absorbing function (3.2.1), we again consider the eigenvalue problem (3.2.10) at $|\xi| < M - \delta$ using Dirichlet boundary conditions (3.2.3) but without the waveguide. Therefore, we set $q(\xi) = q_\infty \equiv \text{const}$ for $-M < \xi < M$, such that the discrete spectrum disappears. Assuming a damping $\Delta_0 = 0.1$, the location of complex eigenvalues $\lambda \in \tilde{\mathcal{L}}_C$ is plotted in Figure 3-6.

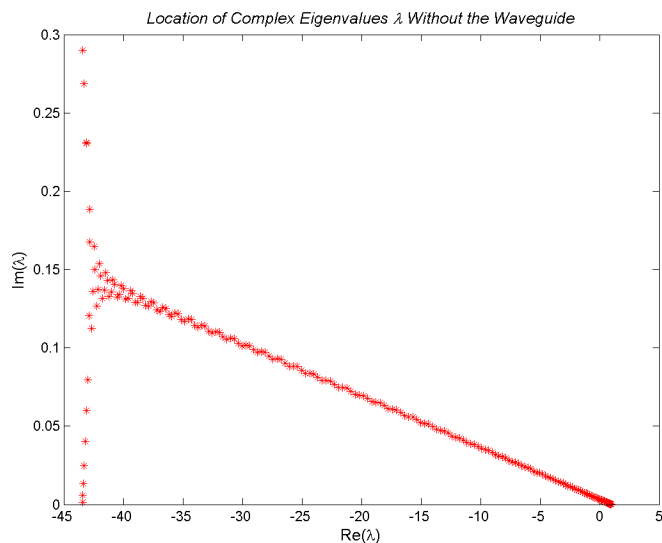


Figure 3-6. Location of complex eigenvalues λ without the waveguide but with damping $\Delta_0 = 0.1$.

From Figure 3-6, we observe that without the presence of the waveguide but with the presence of the linear absorption function (3.2.1), $\tilde{\mathcal{L}}_C$ consists of two distinct branches. Let us denote the lower branch as $\tilde{\mathcal{L}}_{CL}$ and the upper branch as $\tilde{\mathcal{L}}_{CU}$. We shall identify the eigenvectors Φ_j for eigenvalues at $\tilde{\mathcal{L}}_{CL}$ and $\tilde{\mathcal{L}}_{CU}$. Eigenvectors Φ_j

with corresponding eigenvalues $\lambda_L \in \tilde{\mathcal{L}}_{C_L}$ of the lower branch are shown in Figure 3-7(a).

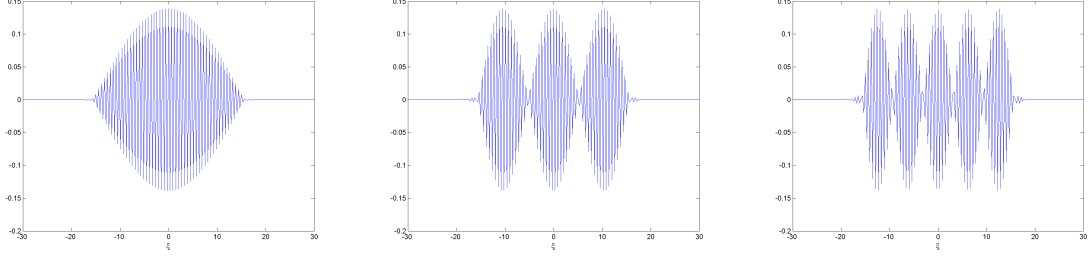


Figure 3-7(a). Three numerical eigenvectors localized in the gap of the absorbing layer: $|\xi| < M - \delta = 15$.

From 3-7(a), we observe that for eigenvalues λ_L on the lower branch $\tilde{\mathcal{L}}_{C_L}$, the corresponding eigenvectors $\Phi_{\mathbf{j}}$ are localized in the gap of the absorbing layer: $|\xi| < M - \delta = 15$. Therefore, eigenvalues λ_L represent radiation and edge modes trapped by the absorbing layer. Each eigenvalue is double and the second eigenvector corresponds to a radiation mode propagating in the opposite direction. Eigenvectors $\Phi_{\mathbf{j}}$ corresponding to eigenvalues $\lambda_U \in \tilde{\mathcal{L}}_{C_U}$ of the upper branch are shown in Figure 3-7(b).

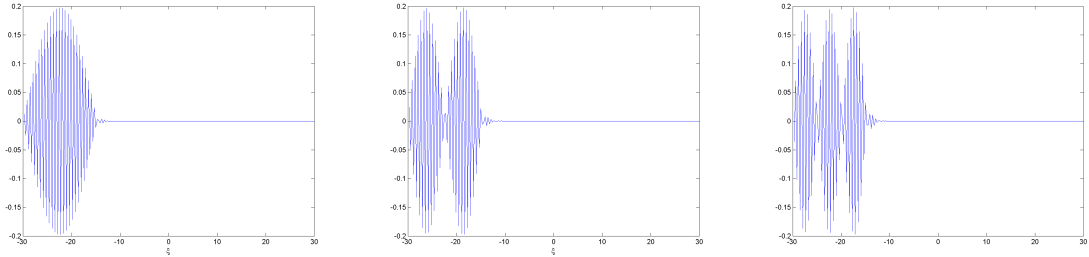


Figure 3-7(b). Three numerical eigenvectors localized in the absorbing layer: $|\xi| > M - \delta = 15$.

From 3-7(b), we observe that for eigenvalues λ_U on the upper branch $\tilde{\mathcal{L}}_{C_U}$, the corresponding eigenvectors $\Phi_{\mathbf{j}}$ are localized in the absorbing layer: $|\xi| > M - \delta = 15$.

Therefore, eigenvalues λ_U represent radiation and edge modes escaping the absorbing layer. Each eigenvalue is double and the second eigenvector is reflected about $\xi = 0$. We explain the reduction of radiation, seen in Figure 3-5(b), by zero coefficients $\{a_j, b_j\}$ for eigenvalues λ_U on the upper branch $\tilde{\mathcal{L}}_{C_U}$. Indeed, the energy density P_j is essentially zero for all eigenvalues λ_U , seen in Figure 3-4(a) and (b). Therefore, we have shown that Ψ^\pm is very small for $|\xi| > M - \delta = 15$, seen in Figure 3-5(b). We conclude numerically, that the splitting of eigenvalues of $\lambda \in \tilde{\mathcal{L}}_C$ occurs due to the gap in piecewise linear absorption function (3.2.1). Now we will be varying the damping coefficient Δ_0 and study changes in the two branches $\lambda_L \in \tilde{\mathcal{L}}_{C_L}$ and $\lambda_U \in \tilde{\mathcal{L}}_{C_U}$. Figure 3-8(a) and 3-8(b) show the location of the complex eigenvalue $\lambda \in \tilde{\mathcal{L}}_C$ for $\Delta_0 = 1$ and $\Delta_0 = 10$.

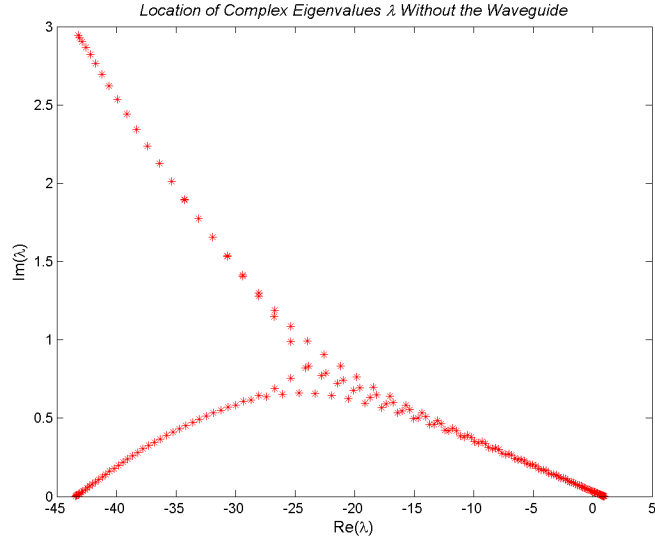


Figure 3-8(a). Location of complex eigenvalues λ without the waveguide but with damping $\Delta_0 = 1$.

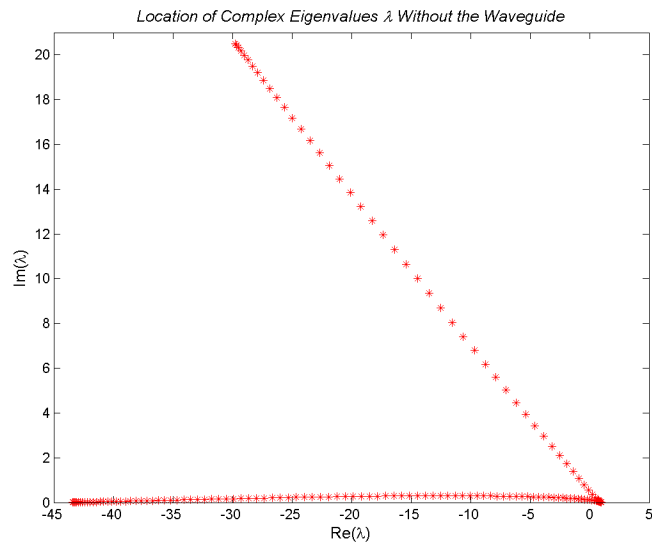


Figure 3-8(b). Location of complex eigenvalues λ without the waveguide but with damping $\Delta_0 = 10$.

Referring to Figure 3-6 and comparing with Figure 3-8(a) and 3-8(b), we conclude that $\text{Im}(\lambda_U)$ increases on the upper branch $\tilde{\mathcal{L}}_{C_U}$ and $\text{Im}(\lambda_L)$ decreases on the lower branch $\tilde{\mathcal{L}}_{C_L}$, as the damping coefficient Δ_0 increases. Also, the splitting boundary moves from the left end to the right end of the spectrum, which is $\lambda = q_\infty$.

Chapter 4

Summary

In this project, we have successfully developed a computational algorithm for solving the stationary *Maxwell* equation at the interface between two planar waveguides. The algorithm operated with arbitrary refractive index profiles on both sides of the interface and with arbitrary incident electric field from one side. The algorithm computed the reflection and transmission coefficients for trapped waveguide modes, radiation waves and edge states localized at the interface. To reduce the presence of radiating waves from artificial boundary-reflected waveguides, we introduced absorbing layers into the computational domain and observed localization of radiation and edge modes at the center of the waveguides.

Opposing traditional approaches to similar problems, based in time-domain computations, we worked in a frequency domain. As a result, our numerical algorithm was based on the finite-difference frequency-domain (FDFD) method, rather than the finite-difference time-domain (FDTD) method [18][23][26]. Using the FDFD method, we were able to describe a new technique for the simulation of electromagnetic wave propagation at the interface between two planar waveguides. In comparison with the

FDTD method, the FDFD method required less computation and storage, yet produced a convergent algorithm with accurate results. Our resulting algorithm is the ideal candidate for implementation in parallel computing.

In chapter 1, we reduced the wave propagation problem given by the stationary *Maxwell* equation (1.1.13), to the spectral problem (1.4.4), for the one-dimensional *Schrodinger* operator. We also considered the energy flux through the interface of two planar waveguides, given by *Poynting's* theorem (1.5.1).

In chapter 2, we used the FDFD method in order to solve the spectral problem (1.4.4) for the one-dimensional *Schrodinger* operator. We verified that the spectral problem (1.4.4), consisted of strictly real eigenvalues λ and were able to differentiate the locations of waveguide modes of the discrete spectrum from radiation and edge modes of the continuous spectrum. The FDFD method enabled us to develop a numerical algorithm based on spectral decompositions for the one-dimensional Schrodinger operators, diagonalization formulae, and linear algebra solutions. The result of this algorithm was a set of linear equations at the interface between two planar waveguides, with a solution that produced approximations of reflected, incident and transmitted wave intensities. Using such approximations enabled us to depict three-dimensional visualizations of the electric and magnetic field distributions in each waveguide. Numerically, we also verified the law of conservation of energy across the interface.

In chapter 3, using the FDFD method, we extend our algorithm with an absorbing layer; to absorb outgoing waves from artificial boundary-reflected waveguides. This modified algorithm from chapter 2, no longer relied on orthogonal spectral decompositions and projection operators. To introduce a thin absorbing layer on the boundaries of the computational domain, a complexification of transverse was used.

The resulting spectral problem (1.4.4) for the *Schrodinger* operator was transformed to the complex plane $x \in \mathbb{C}$, inducing a spectral deformation of the eigenvalues λ of the continuous spectrum. Using numerical approximations, we were able to simultaneously solve a set of algebraic equations at the interface between two planar waveguides. From the numerical solutions, we displayed an overview of the electric and magnetic field distributions in each waveguide. Such visualizations enabled us to observe the effective absorption of outgoing waves from artificial boundary-reflected waveguides.

Appendix A: Numerical Code from Chapter 2

This is the MATLAB script, following the algorithm presented in chapter 2, used to generate Table 2-2, Figure 2-1(a) and 2-1(b) of section 2.7.1:

```
%*****  
%*****  
% Clayton Garrett Webster  
% M.Sc Project  
%Program:  realalgorithm_271_RT.m  
%Boundary Conditions:  Periodic  
%*****  
%*****  
  
    clc  
    clear all;  
    counter=0;  
for a_2=1:0.01:10  
    counter=counter+1;  
    L=30; LZ=30; N=200; P=200; Q=2*P; M=2*N;  
    h=L/N; g=LZ/P;  
    a_1=1.0;  
    Q_1=1.0; Q_2=2.0; Q_3=1.0; Q_4=2.0;  
    c_0 = 1;  
    A_1=zeros (M,M); A_1(1,M)=1/h^2; A_1(1,2)=1/h^2;  
    A_1(M,1)=1/h^2; A_1(M,M-1)=1/h^2;  
    A_2=zeros (M,M); A_2(1,M)=1/h^2; A_2(1,2)=1/h^2;  
    A_2(M,1)=1/h^2; A_2(M,M-1)=1/h^2;
```



```

%*****
%CONSTRUCTION OF MATRIX A_1 to the LEFT of the INTERFACE
%*****
    x=-L+h:h:L;
    x_0=-L;
    for n =1:1:M
        x_n=-L+n*h;
        if x_n<-a_1 | x_n>a_1
            q_n=Q_1;
        else
            q_n=Q_2;
        end
        A_1(n,n)=-2/h^2 + q_n;
    end
    for n=2:1:M-1
        A_1(n,n-1)=1/h^2;
        A_1(n,n+1)=1/h^2;
    end
    [V_1,D_1]=eig(A_1);
%*****
%CONSTRUCTION OF MATRIX A_2 to the RIGHT of the INTERFACE
%*****
    for t=1:1:M
        x_t=-L+t*h;
        if x_t<-a_2 | x_t>a_2
            q_t=Q_3;
        else
            q_t=Q_4;
        end
        A_2(t,t)=-2/h^2 + q_t;
    end
    for t=2:1:M-1
        A_2(t,t-1)=1/h^2;
        A_2(t,t+1)=1/h^2;
    end
    [V_2,D_2]=eig(A_2);
%*****
%INTERMEDIATE MATRIX CALCULATIONS
%*****

```

```

D_1_root=sqrt(D_1); D_2_root=sqrt(D_2);
eigenvalue1=diag(D_1); eigenvalue2=diag(D_2);
index1=find(eigenvalue1>0);
for k=1:1:length(index1)
    eigenvalue_1(k)=eigenvalue1(index1(k));
end
Eigenvalue1=transpose(eigenvalue_1);
index2=find(eigenvalue2>0);
for k=1:1:length(index2)
    eigenvalue_2(k)=eigenvalue2(index2(k));
end
Eigenvalue2=transpose(eigenvalue_2);
Grammian_21=V_2'*V_1; Grammian_11=V_1'*V_1;
Grammian_22=V_2'*V_2;
%*****
%SOLVING THE MATRIX SYSTEM Ba=c for the vectors a and b
%*****
B=D_2_root*Grammian_21 + Grammian_21*D_1_root;
C=-c_0*(D_2_root*Grammian_21(:,M)-D_1_root(M,M)*Grammian_21(:,M));
a=inv(B)*C; c=zeros(M,1); c(M)=c_0;
b=Grammian_21*a + Grammian_21*c;
for k=1:1:length(index1);
    a_1(k)=a(index1(k));
end
a1=transpose(a_1);
for k=1:1:length(index1)
    c_1(k)=c(index1(k));
end
c1=transpose(c_1);
for k=1:1:length(index2)
    b_1(k)=b(index2(k));
end
b1=transpose(b_1);
%*****
%CONSERVATION OF ENERGY RELATION AND FIGURES
%*****
I_reflected= 2*sum(sqrt(diag(Eigenvalue1))*abs(a1).^2);
I_incident=2*sum(sqrt(diag(Eigenvalue1))*abs(c1).^2);
I_transmitted=2*sum(sqrt(diag(Eigenvalue2))*abs(b1).^2);
R=I_reflected/I_incident;

```

```

    T=I_transmitted/I_incident;
    CHECK = R+T;  R_vector(counter)=R;  T_vector(counter)=T;
    tau(counter)=a_2;
end
figure(1);
    fig1=plot(tau,R_vector)
    set(fig1,'Linewidth',2)
    set(fig1,'Color','r')
    xlabel('rho^+', 'FontSize', 12)
    ylabel('Reflectance (R)', 'FontSize', 12)
    title('Reflectance versus rho^+', 'FontSize', 12)
figure(2);
    fig2=plot(tau, T_vector)
    set(fig2,'Linewidth',2)
    set(fig2,'Color','b')
    xlabel('rho^+', 'FontSize', 12)
    ylabel('Transmittance (T)', 'FontSize', 12)
    title('Transmittance versus rho^+', 'FontSize', 12)
%*****
%THE END
%*****

```

This is the MATLAB script, following the algorithm presented in chapter 2, used to generate Figure 2.2, 2.3, 2.4(a) and 2.4(b) of section 2.7.1:

```

%*****
%*****
% Clayton Garrett Webster
% M.Sc Project
%Program:  realalgorithm_271.m
%Boundary Conditions:  Periodic
%*****
%*****
    clc
    clear all;
    L=30; LZ=30; N=200; P=200; Q=2*P; M=2*N;
    h=L/N; g=LZ/P; a_1=1.0; a_2=2.0;
    Q_1=1.0; Q_2=2.0; Q_3=1.0; Q_4=2.0;
    A_1=zeros (M,M); A_1(1,M)= 1/h^2; A_1(1,2)= 1/h^2;
    A_1(M,1)=1/h^2; A_1(M,M-1)=1/h^2;
    A_2=zeros (M,M); A_2(1,M)=1/h^2; A_2(1,2)=1/h^2;
    A_2(M,1)=1/h^2; A_2(M,M-1)=1/h^2;
    c_0 = 1;
%*****
%*****
%CONSTRUCTION OF MATRIX A_1 to the LEFT of the INTERFACE
%*****
    x=-L+h:h:L;
    x_0=-L;
    for n=1:1:M
        x_n=-L+n*h;
        if x_n<-a_1 | x_n>a_1
            q_n=Q_1;
        else
            q_n=Q_2;
        end
        A_1(n,n)=-2/h^2 + q_n;
    end
    for n=2:1:M-1
        A_1(n,n-1)=1/h^2;
        A_1(n,n+1)=1/h^2;
    end
end

```

```

[V_1,D_1]=eig(A_1);
%*****
%CONSTRUCTION OF MATRIX A_2 to the RIGHT of the INTERFACE
%*****
for t=1:1:M
    x_t=-L+t*h;
    if x_t<-a_2 | x_t>a_2
        q_t=Q_3;
    else
        q_t=Q_4;
    end
    A_2(t,t)=-2/h^2 + q_t;
end
for t=2:1:M-1
    A_2(t,t-1)=1/h^2;
    A_2(t,t+1)=1/h^2;
end
[V_2,D_2]=eig(A_2);
%*****
%INTERMEDIATE MATRIX CALCULATIONS
%*****
D_1_root=sqrt(D_1); D_2_root=sqrt(D_2);
eigenvalue1=diag(D_1); eigenvalue2=diag(D_2);
index1=find(eigenvalue1>0);
for k=1:1:length(index1)
    eigenvalue_1(k)=eigenvalue1(index1(k));
end
Eigenvalue1=transpose(eigenvalue_1);
index2 = find(eigenvalue2>0);
for k=1:1:length(index2)
    eigenvalue_2(k)=eigenvalue2(index2(k));
end
Eigenvalue2=transpose(eigenvalue_2);
Grammian_21=V_2'*V_1; Grammian_11=V_1'*V_1;
Grammian_22=V_2'*V_2;
%*****
%SOLVING THE MATRIX SYSTEM Ba=c for the vectors a and b
%*****
B=D_2_root*Grammian_21 + Grammian_21*D_1_root;
C=-c_0*(D_2_root*Grammian_21(:,M)-D_1_root(M,M)*Grammian_21(:,M));

```

```

a=inv(B)*C; c=zeros(M,1); c(M) = c_0;
b=Grammian_21*a + Grammian_21*c;
for k=1:1:length(index1)
    a_1(k)=a(index1(k));
end
a1=transpose(a_1);
for k=1:1:length(index1)
    c_1(k)=c(index1(k));
end
c1=transpose(c_1);
for k=1:1:length(index2)
    b_1(k)=b(index2(k));
end
b1=transpose(b_1);
%*****
%FIGURES: spectrum
%*****
figure(1); plot (Eigenvalue2, (2*sqrt(Eigenvalue2)).*(abs(b1).^2), '*');
    xlabel('Eigenvalue lambda^+', 'FontSize', 12);
    ylabel('Energy Density E_ j ^ + ', 'FontSize', 12);
    title('Energy Spectrum for Transmitted Radiation Modes', 'FontSize', 12);
figure(2); plot (Eigenvalue1, (2*sqrt(Eigenvalue1)).*(abs(a1).^2), '*');
    xlabel('Eigenvalue lambda^- ', 'FontSize', 12);
    ylabel('Energy Density E_ j ^ - ', 'FontSize', 12);
    title('Energy Spectrum for Reflected Radiation Modes', 'FontSize', 12);
%*****
%CONSERVATION OF ENERGY RELATION
%*****
I_reflected=2*sum(sqrt(diag(Eigenvalue1))*abs(a1).^2)
I_incident=2*sum(sqrt(diag(Eigenvalue1))*abs(c1).^2)
I_transmitted=2*sum(sqrt(diag(Eigenvalue2))*abs(b1).^2)
R=I_reflected/I_incident;
T=I_transmitted/I_incident;
CHECK=R+T;
S1=V_1*a +V_1*c;
S2=V_1*(-i*D_1_root*a) + V_1*(i*D_1_root*c);
S_left=sum(conj(S1).*S2);
S3=V_2*b;
S4=V_2*(i*D_2_root*b);
S_right=sum(conj(S3).*S4);

```

```

    S_sum=real(S_left) + real(S_right);
%*****
%CONSTRUCTION OF SOLUTION MATRICES
%*****
    z=-LZ : g : LZ; Psi1=zeros(M,P+1); Psi2=zeros(M,P);
    for k=1 : (P+1)
        E_1=diag(exp(-i*diag(D_1_root)*z(k)));
    Sol_Matrix_1=V_1*(diag(a)*E_1 + diag(c)*inv(E_1));
    Psi1(:,k)=sum(Sol_Matrix_1')';
    end
    for k=(P+2) : Q+1
        E_2=diag(exp(i*diag(D_2_root)*z(k)));
    Sol_Matrix_2=V_2*diag(b)*E_2;
    Psi2(:,k-P-1)=sum(Sol_Matrix_2')';
    end
%*****
%CONSTRUCTION OF THE 3-D WAVEGUIDE PLOT
%*****
    [Z,X] = meshgrid(z,x);
    Psi = [Psi1, Psi2];
figure(3);
    surf(Z,X,abs(Psi).^2);
    colorbar;
    view(0,75);
    shading interp;
    lightangle(-45,30);
    set(findobj(gca, 'type', 'surface'),...
        'FaceLighting', 'phong',...
        'AmbientStrength', .3, 'DiffuseStrength', .8,...
        'SpecularStrength', .9, 'SpecularExponent', 25,...
        'BackFaceLighting', 'unlit');
    xlabel('z', 'FontSize', 12);
    ylabel('x', 'FontSize', 12);
    zlabel(' Amplitude of Wave Solution', 'FontSize', 12);
    title('Numerical Representation of Waveguide', 'FontSize', 12);
figure(4);
    surf(Z,X,abs(Psi).^2);
    view(0,0);
    shading interp;
    lightangle(0,-90);

```

```
set(findobj(gca, 'type', 'surface'),...
    'FaceLighting', 'phong',...
    'AmbientStrength',.3,'DiffuseStrength',.8,...
    'SpecularStrength',.9,'SpecularExponent',25,...
    'BackFaceLighting', 'unlit');
xlabel('z', 'FontSize', 12);
ylabel('x', 'FontSize', 12);
zlabel('Amplitude of Wave Solution', 'FontSize', 12);
title('Numerical Representation of Radiation from Waveguide', 'FontSize', 12);
%*****
%THE END
%*****
```


This is the MATLAB script, following the algorithm presented in chapter 2, used to generate Table 2-3 and Figure 2-5 of section 2.7.2:

```

%*****
%*****
% Clayton Garrett Webster
% M.Sc Project
%Program:  realalgorithm_272_RT2.m
%Boundary Conditions:  Periodic
%*****
%*****
    clc
    clear all;
    counter=0;
for Q_4=1:0.01:10
counter=counter+1;
    L=30; LZ=30; N=100; P=100; Q=2*P; M=2*N;
    h=L/N; g=LZ/P; a_1=1.0; a_2=2.0;
    Q_1=1.0; Q_2=2.0; Q_3=1.0;
    A_1=zeros (M,M); A_1(1,M)=1/h^2; A_1(1,2)=1/h^2;
    A_1(M,1)= 1/h^2; A_1(M,M-1)=1/h^2;
    A_2=zeros (M,M); A_2(1,M)=1/h^2; A_2(1,2)=1/h^2;
    A_2(M,1)=1/h^2; A_2(M,M-1)=1/h^2;
    c_0=1;
%*****
%*****
%CONSTRUCTION OF MATRIX A_1 to the LEFT of the INTERFACE
%*****
%*****
    x=-L+h:h:L; x_0=-L;
    for n=1:1:M
        x_n=-L+n*h;
        if x_n<-a_1 | x_n>a_1
            q_n=Q_1;
        else
            q_n=Q_2;
        end
        A_1(n,n)=-2/h^2 + q_n;
    end
    for n=2:1:M-1
        A_1(n,n-1)=1/h^2;

```

```

        A_1(n,n+1)=1/h^2;
    end
    [V_1,D_1]=eig(A_1);
%*****
%CONSTRUCTION OF MATRIX A_2 to the RIGHT of the INTERFACE
%*****
    for t=1:1:M
        x_t=-L+t*h;
        if x_t<-a_2 | x_t>a_2
            q_t=Q_3;
        else
            q_t=Q_4;
        end
        A_2(t,t)=-2/h^2 + q_t;
    end
    for t=2:1:M-1
        A_2(t,t-1)=1/h^2;
        A_2(t,t+1)=1/h^2;
        [V_2,D_2]=eig(A_2);
%*****
%INTERMEDIATE MATRIX CALCULATIONS
%*****
        D_1_root=sqrt(D_1); D_2_root=sqrt(D_2);
        eigenvalue1=diag(D_1);
        eigenvalue2=diag(D_2);
        index1=find(eigenvalue1>0);
        for k=1:1:length(index1)
            eigenvalue_1(k)=eigenvalue1(index1(k));
        end
        Eigenvalue1=transpose(eigenvalue_1);
        index2=find(eigenvalue2>0);
        for k=1:1:length(index2)
            eigenvalue_2(k)=eigenvalue2(index2(k));
        end
        Eigenvalue2=transpose(eigenvalue_2);
        Grammian_21=V_2'*V_1; Grammian_11=V_1'*V_1;
        Grammian_22=V_2'*V_2;
%*****
%SOLVING THE MATRIX SYSTEM Ba=c for the vectors a and b
%*****

```

```

B=D_2_root*Grammian_21 + Grammian_21*D_1_root;
C=-c_0*(D_2_root*Grammian_21(:,M)-D_1_root(M,M)*Grammian_21(:,M));
a=inv(B)*C; c=zeros(M,1); c(M)=c_0;
b=Grammian_21*a + Grammian_21*c;
for k=1:1:length(index1)
    a_1(k)=a(index1(k));
end
a1=transpose(a_1);
for k=1:1:length(index1)
    c_1(k)=c(index1(k));
end
c1=transpose(c_1);
for k=1:1:length(index2)
    b_1(k)=b(index2(k));
end
b1=transpose(b_1);
%*****
%CONSERVATION OF ENERGY RELATION AND FIGURES
%*****
I_reflected=2*sum(sqrt(diag(Eigenvalue1))*abs(a1).^2);
I_incident=2*sum(sqrt(diag(Eigenvalue1))*abs(c1).^2);
I_transmitted=2*sum(sqrt(diag(Eigenvalue2))*abs(b1).^2);
R=I_reflected/I_incident;
T=I_transmitted/I_incident;
CHECK=R+T;
R_vector(counter)=R;
T_vector(counter)=T;
di(counter)=Q_4;
end
figure(1);
fig1=plot(di,R_vector,di, T_vector)
set(fig1,'Linewidth',2)
set(fig1,'Color','r';'b')
xlabel('q^+_0', 'FontSize', 12)
legend(fig1,'R','T')
title('Reflectance and Transmittance versus q^+_0', 'FontSize', 12)
%*****
%THE END
%*****

```

This is the MATLAB script, following the algorithm presented in chapter 2, used to generate Figure 2.6, 2.7, 2.8(a) and 2.8(b) of section 2.7.2:

```

%*****
%*****
% Clayton Garrett Webster
% M.Sc Project
%Program:  realalgorithm_272.m
%Boundary Conditions:  Periodic
%*****
%*****
    clc
    clear all;
    L=30; LZ=30; N=100; P=100; Q=2*P; M=2*N;
    h=L/N; g=LZ/P; a_1=1.0; a_2=2.0;
    Q_1=1.0; Q_2=2.0; Q_3=1.0; Q_4=4.0
    A_1=zeros (M,M); A_1(1,M)=1/h^2; A_1(1,2)=1/h^2;
    A_1(M,1)=1/h^2; A_1(M,M-1)=1/h^2;
    A_2=zeros (M,M); A_2(1,M)=1/h^2; A_2(1,2)=1/h^2;
    A_2(M,1)=1/h^2; A_2(M,M-1)=1/h^2;
    c_0=1;
%*****
%*****
%CONSTRUCTION OF MATRIX A_1 to the LEFT of the INTERFACE
%*****
%*****
    x=-L+h:h:L;
    x_0=-L;
    for n = 1:1:M
        x_n=-L+n*h;
        if x_n<-a_1 | x_n>a_1
            q_n=Q_1;
        else
            q_n=Q_2;
        end
        A_1(n,n)=-2/h^2 + q_n;
    end
    for n=2:1:M-1
        A_1(n,n-1)=1/h^2;
        A_1(n,n+1)=1/h^2;
    end
end

```

```

[V_1,D_1]=eig(A_1);
%*****
%CONSTRUCTION OF MATRIX A_2 to the RIGHT of the INTERFACE
%*****
for t=1:1:M
    x_t=-L+t*h;
    if x_t<-a_2 | x_t>a_2
        q_t=Q_3;
    else
        q_t=Q_4;
    end
    A_2(t,t)=-2/h^2 + q_t;
end
for t=2:1:M-1
    A_2(t,t-1)=1/h^2;
    A_2(t,t+1)=1/h^2;
end
[V_2,D_2]=eig(A_2);
%*****
%INTERMEDIATE MATRIX CALCULATIONS
%*****
D_1_root=sqrt(D_1); D_2_root = sqrt(D_2);
eigenvalue1=diag(D_1); eigenvalue2 = diag(D_2);
index1=find(eigenvalue1>0);
for k=1:1:length(index1)
    eigenvalue_1(k)=eigenvalue1(index1(k));
end
Eigenvalue1=transpose(eigenvalue_1);
index2=find(eigenvalue2>0);
for k=1:1:length(index2)
    eigenvalue_2(k)=eigenvalue2(index2(k));
end
Eigenvalue2=transpose(eigenvalue_2);
Grammian_21=V_2'*V_1; Grammian_11=V_1'*V_1;
Grammian_22=V_2'*V_2;
%*****
%SOLVING THE MATRIX SYSTEM Ba=c for the vectors a and b
%*****
B=D_2_root*Grammian_21 + Grammian_21*D_1_root;
C=-c_0*(D_2_root*Grammian_21(:,M)-D_1_root(M,M)*Grammian_21(:,M));

```

```

a=inv(B)*C; c=zeros(M,1); c(M)=c_0;
b=Grammian_21*a + Grammian_21*c;
for k=1:1:length(index1)
    a_1(k)=a(index1(k));
end
a1=transpose(a_1);
for k=1:1:length(index1)
    c_1(k)=c(index1(k));
end
c1=transpose(c_1);
for k=1:1:length(index2)
    b_1(k)=b(index2(k));
end
b1=transpose(b_1);
%*****
%FIGURES: spectrum
%*****
figure(1); plot (Eigenvalue2, (2*sqrt(Eigenvalue2)).*(abs(b1).^2), '*');
    xlabel('Eigenvalue lambda^+', 'FontSize', 12);
    ylabel('Energy Density E_ j ^ + ', 'FontSize', 12);
    title('Energy Spectrum for Transmitted Radiation Modes', 'FontSize', 12);
figure(2); plot (Eigenvalue1, (2*sqrt(Eigenvalue1)).*(abs(a1).^2), '*');
    xlabel('Eigenvalue lambda^- ', 'FontSize', 12);
    ylabel('Energy Density E_ j ^ - ', 'FontSize', 12);
    title('Energy Spectrum for Reflected Radiation Modes', 'FontSize', 12);
%*****
%CONSERVATION OF ENERGY RELATION
%*****
I_reflected=2*sum(sqrt(diag(Eigenvalue1))*abs(a1).^2)
I_incident=2*sum(sqrt(diag(Eigenvalue1))*abs(c1).^2)
I_transmitted=2*sum(sqrt(diag(Eigenvalue2))*abs(b1).^2)
R=I_reflected/I_incident;
T=I_transmitted/I_incident;
CHECK = R+T;
S1=V_1*a +V_1*c;
S2=V_1*(-i*D_1_root*a) + V_1*(i*D_1_root*c);
S_left=sum(conj(S1).*S2);
S3=V_2*b;
S4=V_2*(i*D_2_root*b);
S_right=sum(conj(S3).*S4);

```

```

    S_sum=real(S_left) + real(S_right);
%*****
%CONSTRUCTION OF SOLUTION MATRICES
%*****
    z=-LZ : g : LZ;
    Psi1=zeros(M,P+1);
    Psi2=zeros(M,P);
    for k=1 : (P+1)
        E_1=diag(exp(-i*diag(D_1_root)*z(k)));
        Sol_Matrix_1=V_1*(diag(a)*E_1 + diag(c)*inv(E_1));
    Psi1(:,k)=sum(Sol_Matrix_1)';
    end
    for k=(P+2) : Q+1
        E_2=diag(exp(i*diag(D_2_root)*z(k)));
        Sol_Matrix_2=V_2*diag(b)*E_2;
    Psi2(:,k-P-1)=sum(Sol_Matrix_2)';
    end
%*****
%CONSTRUCTION THE 3-D PLOT OF THE WAVE-GUIDE
%*****
    [Z,X]=meshgrid(z,x);
    Psi=[Psi1, Psi2];
    figure(3); surf(Z,X,abs(Psi).^2);
    colorbar;
    view(0,75);
    shading interp;
    lightangle(-45,30);
    set(findobj(gca, 'type', 'surface'),...
        'FaceLighting', 'phong',...
        'AmbientStrength', .3, 'DiffuseStrength', .8,...
        'SpecularStrength', .9, 'SpecularExponent', 25,...
        'BackFaceLighting', 'unlit');
    xlabel('z', 'FontSize', 12);
    ylabel('x', 'FontSize', 12);
    zlabel(' Amplitude of Wave Solution', 'FontSize', 12);
    title('Numerical Representation of Waveguide', 'FontSize', 12);
    figure(4);
    surf(Z,X,abs(Psi).^2);
    view(0,0);
    shading interp;

```

```
lightangle(0,-90);
set(findobj(gca, 'type', 'surface'),...
    'FaceLighting', 'phong',...
    'AmbientStrength',.3,'DiffuseStrength',.8,...
    'SpecularStrength',.9,'SpecularExponent',25,...
    'BackFaceLighting', 'unlit');
xlabel('z', 'FontSize', 12);
ylabel('x', 'FontSize', 12);
zlabel('Amplitude of Wave Solution', 'FontSize', 12);
title('Numerical Representation of Radiation from Waveguide', 'FontSize', 12);
%*****
%THE END
%*****
```


Appendix B: Numerical Code from Chapter 3

This is the MATLAB script, following the algorithm presented in chapter 3, used to generate all figures in section 3.5:

```
%*****
%*****
% Clayton Garrett Webster
% M.Sc Project
%Program:  absorbinglayer_algorithm.m
%Boundary Conditions:  Dirichlet
%*****
%*****

    clc
    clear all;
    L=30; LZ=30; N=100; P=100; Q=2*P; M=2*N-1;
    h=L/N; g=LZ/P; a_1=1.0; a_2=2.0;
    Q_1=1.0; Q_2=2.0; Q_3=1.0;
    Q_4=4.0;
    A_1=zeros (M,M); A_2=zeros (M,M);
    c_0=1;

%*****
%*****
%ABSORBING LAYER IN COMPLEX TRANSFORMATION
%*****
%*****

    delta=50*h;
    Delta_0=0.1;
    Delta=-Delta_0/delta;

%*****
%*****
%CONSTRUCTION OF MATRIX A_1 to the LEFT of the INTERFACE
%*****
%*****
```

```

xi=-L+h:h:L-h;
for n=1:1:M
    if xi(n)<-a_1 | xi(n)>a_1
        q_n=Q_1;
    else
        q_n=Q_2;
    end
    if (xi(n)<=(L-delta)) & (xi(n)>=(-L+delta))
        C_n=1;
    else
        C_n=1-i*Delta;
    end
    A_1(n,n)=-2/(C_n*h^2) + q_n;
    if n == 1
        A_1(1,2)=1/(C_n*h^2);
    elseif n == M
        A_1(M,M-1)=1/(C_n*h^2);
    else
        A_1(n,n-1)=1/(C_n*h^2);
        A_1(n,n+1)=1/(C_n*h^2);
    end
end
[V_1,D_1]=eig(A_1);
%*****
%CONSTRUCTION OF MATRIX A_2 to the RIGHT of the INTERFACE
%*****
for t=1:1:M
    if xi(t)<-a_2 | xi(t)>a_2
        q_t=Q_3;
    else
        q_t=Q_4;
    end
    if (xi(t)<=(L-delta)) & (xi(t)>=(-L+delta))
        C_t = 1;
    else
        C_t = 1-i*Delta;
    end
    A_2(t,t)=-2/(C_t*h^2) + q_t;
    if t == 1
        A_2(1,2)=1/(C_t*h^2);

```

```

        elseif t == M
            A_2(M,M-1)=1/(C_t*h^2);
        else
            A_2(t,t-1)=1/(C_t*h^2);
            A_2(t,t+1)=1/(C_t*h^2);
        end
    end

    [V_2,D_2]=eig(A_2);
    abs_norm=norm((A_2*V_2) - (D_2*V_2));
%*****
%INTERMEDIATE MATRIX CALCULATIONS and SORTING OF
%EIGENVALUES
%*****
    eigenvalue1=diag(D_1);  eigenvalue2=diag(D_2);
    eigenvalue1_real=real(eigenvalue1);
    eigenvalue1_imaginary=imag(eigenvalue1);
    eigenvalue2_real=real(eigenvalue2);
    eigenvalue2_imaginary=imag(eigenvalue2);
    [x1_real, index_1]=sort(eigenvalue1_real);
    [x2_real, index_2]=sort(eigenvalue2_real);
    x1_imaginary=eigenvalue1_imaginary(index_1);
    x2_imaginary=eigenvalue2_imaginary(index_2);
    V_1_sort=V_1(:,index_1);  V_2_sort=V_2(:,index_2);
    D_1_sort=D_1(:,index_1);  D_2_sort=D_2(:,index_2);
    for p=1:1:M
        eigenvalue1_sort(p)=D_1_sort(find(D_1_sort(:,p)), p);
        eigenvalue2_sort(p)=D_2_sort(find(D_2_sort(:,p)), p);
    end
    EIGENVALUES1=transpose(eigenvalue1_sort);
    EIGENVALUES2=transpose(eigenvalue2_sort);
    D_1_root=zeros(M,M);
    D_2_root=zeros(M,M);
    for s=1:1:M
        D_1_diag(s,s)=EIGENVALUES1(s);
        D_2_diag(s,s)=EIGENVALUES2(s);
    end
    D_1_root=sqrt(D_1_diag);  D_2_root=sqrt(D_2_diag);
    R_EIG1=real(EIGENVALUES1);  R_EIG2=real(EIGENVALUES2);
    index1=find(R_EIG1>0);
    for k=1:1:length(index1)

```

```

    r_eigenvalue1(k)=R_EIG1(index1(k));
end
R_Eigenvalue1=transpose(r_eigenvalue1);
index2=find(R_EIG2>0);
for k=1:1:length(index2)
    r_eigenvalue2(k)=R_EIG2(index2(k));
end
R_Eigenvalue2=transpose(r_eigenvalue2);
%*****
%CONSTRUCT THE MATRIX A THAT SOLVES FOR THE
%COEFFICIENT VECTORS a and b SIMULTANEOUSLY FROM Ax=y
%*****
V1=V_1_sort*D_1_root; V2=V_2_sort*D_2_root;
A=[-V_1_sort, V_2_sort; V1, V2];
y=c_0*[V_1_sort(:,M); D_1_root(M,M)*V_1_sort(:,M)]; x=inv(A)*y;
for r=1:1:M
    a(r)=x(r);
end
a_ref=transpose(a);
for r=M+1:1:2*M
    b(r-M)=x(r);
end
b_trans=transpose(b); c=zeros(M,1); c(M)=c_0;
for k=1:1:length(index1)
    a_1(k)=a(index1(k));
end
a1=transpose(a_1);
for k=1:1:length(index1)
    c_1(k)=c(index1(k));
end
c1=transpose(c_1);
for k=1:1:length(index2)
    b_1(k)=b(index2(k));
end
b1=transpose(b_1);
%*****
%FIGURES: spectrum and location of eigenvalues
%*****
figure(1);
plot (R_EIG2, (2*sqrt(abs(EIGENVALUES2))).*(abs(b_trans).^2), '*');

```

```

    xlabel('Re(lambda^+)', 'FontSize', 12);
    ylabel('Plotting Factor P_j ^ + ', 'FontSize', 12);
    title('Continuous Spectrum for Transmitted Modes', 'FontSize', 12);
figure(2);
    plot (R_EIG1, (2*sqrt(abs(EIGENVALUES1))).*(abs(a_ref).^2), '*');
    xlabel('Re(lambda^-)', 'FontSize', 12);
    ylabel('Plotting Factor P_j ^ - ', 'FontSize', 12);
    title('Continuous Spectrum for Reflected Modes', 'FontSize', 12);
figure(3);
    plot (x1_real, x1_imaginary, '*', 'Color', 'r');
    xlabel('Re(lambda^-)', 'FontSize', 12);
    ylabel('Im(lambda^-)', 'FontSize', 12);
    title('Position of Complex Eigenvalues lambda^-', 'FontSize', 12);
figure(4);
    plot (x2_real, x2_imaginary, '*', 'Color', 'r');
    xlabel('Re(lambda^+)', 'FontSize', 12);
    ylabel('Im(lambda^+)', 'FontSize', 12);
    title('Position of Complex Eigenvalues lambda^+', 'FontSize', 12);
%*****
%CONSTRUCTION OF SOLUTION MATRICES
%*****
    z=-LZ : g : LZ; Psi1=zeros(M,P+1); Psi2=zeros(M,P);
    for k=1 : (P+1)
        E_1=diag(exp(-i*diag(D_1_root)*z(k)));
        Sol_Matrix_1=V_1_sort*(diag(a)*E_1 + diag(c)*inv(E_1));
        Psi1(:,k)=sum(Sol_Matrix_1)';
    end
    for k=(P+2) : Q+1
        E_2=diag(exp(i*diag(D_2_root)*z(k)));
        Sol_Matrix_2=V_2_sort*diag(b)*E_2;
        Psi2(:,k-P-1)=sum(Sol_Matrix_2)';
    end
%*****
%CONSTRUCTION THE 3-D PLOT OF THE WAVE-GUIDE
%*****
    [Z,X]=meshgrid(z,xi); Psi=[Psi1, Psi2];
figure(5);
    surf(Z,X,abs(Psi).^2);
    colorbar;
    view(0,75);

```

```

shading interp;
lightangle(-45,30);
set(findobj(gca, 'type', 'surface'),...
    'FaceLighting', 'phong',...
    'AmbientStrength',.3,'DiffuseStrength',.8,...
    'SpecularStrength',.9,'SpecularExponent',25,...
    'BackFaceLighting','unlit');
xlabel('z', 'FontSize', 12);
ylabel('xi', 'FontSize', 12);
zlabel(' Amplitude of Wave Solution', 'FontSize', 12);
title('Numerical Representation of Waveguide', 'FontSize', 12);
figure(6);
surf(Z,X,abs(Psi).^2);
view(0,0);
shading interp;
lightangle(0,-90);
set(findobj(gca, 'type', 'surface'),...
    'FaceLighting', 'phong',...
    'AmbientStrength',.3,'DiffuseStrength',.8,...
    'SpecularStrength',.9,'SpecularExponent',25,...
    'BackFaceLighting', 'unlit');
xlabel('z', 'FontSize', 12);
ylabel('xi', 'FontSize', 12);
zlabel('Amplitude of Wave Solution', 'FontSize', 12);
title('Numerical Representation of Radiation from Waveguide', 'FontSize', 12);
%*****
%THE END
%*****

```

This is the MATLAB script, following the algorithm presented in chapter 3, used to generate all figures in section 3.6:

```

%*****
%*****
% Clayton Garrett Webster
% M.Sc Project
%Program:  absorbinglayer_algorithm_nowaveguide.m
%Boundary Conditions:  Dirichlet
%*****
%*****
    clc
    clear all;
    L=30; LZ=30; N=100; P=100; Q=2*P; M=2*N-1;
    h=L/N; g=LZ/P; a_1=1.0; a_2=2.0;
    Q_1=1.0; Q_2=1.0; Q_3=1.0;
    Q_4=1.0; %no waveguide
    A_1=zeros (M,M); A_2=zeros (M,M);
    c_0=1;
%*****
%*****
%ABSORBING LAYER IN COMPLEX TRANSFORMATION
%*****
    delta=50*h;
    Delta_0=0.1; % =1, =10
    Delta=-Delta_0/delta;
%*****
%*****
%CONSTRUCTION OF MATRIX A_1 to the LEFT of the INTERFACE
%*****
    xi=-L+h:h:L-h;
    for n=1:1:M
        if xi(n)<-a_1 | xi(n)>a_1
            q_n=Q_1;
            else
            q_n=Q_2;
            end
            if (xi(n)<=(L-delta)) & (xi(n)>=(-L+delta))
                C_n=1;
            else
                C_n=1-i*Delta;
            end
        end
    end

```

```

        end
    A_1(n,n)=-2/(C_n*h^2) + q_n;
        if n == 1
            A_1(1,2)=1/(C_n*h^2);
        elseif n == M
            A_1(M,M-1)=1/(C_n*h^2);
        else
            A_1(n,n-1)=1/(C_n*h^2);
            A_1(n,n+1)=1/(C_n*h^2);
        end
    end

    [V_1,D_1]=eig(A_1);
%*****
%CONSTRUCTION OF MATRIX A_2 to the RIGHT of the INTERFACE
%*****
    for t=1:1:M
        if xi(t)<-a_2 | xi(t)>a_2
            q_t=Q_3;
        else
            q_t=Q_4;
        end
        if (xi(t)<=(L-delta)) & (xi(t)>=(-L+delta))
            C_t = 1;
        else
            C_t = 1-i*Delta;
        end
    A_2(t,t)=-2/(C_t*h^2) + q_t;
        if t == 1
            A_2(1,2)=1/(C_t*h^2);
        elseif t == M
            A_2(M,M-1)=1/(C_t*h^2);
        else
            A_2(t,t-1)=1/(C_t*h^2);
            A_2(t,t+1)=1/(C_t*h^2);
        end
    end

    [V_2,D_2]=eig(A_2);
    abs_norm=norm((A_2*V_2) - (D_2*V_2));

```



```

%*****
%INTERMEDIATE MATRIX CALCULATIONS and SORTING OF
%EIGENVALUES
%*****
eigenvalue1=diag(D_1); eigenvalue2=diag(D_2);
eigenvalue1_real=real(eigenvalue1);
eigenvalue1_imaginary=imag(eigenvalue1);
eigenvalue2_real=real(eigenvalue2);
eigenvalue2_imaginary=imag(eigenvalue2);
[x1_real, index_1]=sort(eigenvalue1_real);
[x2_real, index_2]=sort(eigenvalue2_real);
x1_imaginary=eigenvalue1_imaginary(index_1);
x2_imaginary=eigenvalue2_imaginary(index_2);
V_1_sort=V_1(:,index_1); V_2_sort=V_2(:,index_2);
D_1_sort=D_1(:,index_1); D_2_sort=D_2(:,index_2);
for p=1:1:M
    eigenvalue1_sort(p)=D_1_sort(find(D_1_sort(:,p)), p);
    eigenvalue2_sort(p)=D_2_sort(find(D_2_sort(:,p)), p);
end
EIGENVALUES1=transpose(eigenvalue1_sort);
EIGENVALUES2=transpose(eigenvalue2_sort);
D_1_root=zeros(M,M);
D_2_root=zeros(M,M);
for s=1:1:M
    D_1_diag(s,s)=EIGENVALUES1(s);
    D_2_diag(s,s)=EIGENVALUES2(s);
end
D_1_root=sqrt(D_1_diag); D_2_root=sqrt(D_2_diag);
R_EIG1=real(EIGENVALUES1); R_EIG2=real(EIGENVALUES2);
index1=find(R_EIG1>0);
for k=1:1:length(index1)
    r_eigenvalue1(k)=R_EIG1(index1(k));
end
R_Eigenvalue1=transpose(r_eigenvalue1);
index2=find(R_EIG2>0);
for k=1:1:length(index2)
    r_eigenvalue2(k)=R_EIG2(index2(k));
end
R_Eigenvalue2=transpose(r_eigenvalue2);

```

```

%*****
%CONSTRUCT THE MATRIX A THAT SOLVES FOR THE
%COEFFICIENT VECTORS a and b SIMULTANEOUSLY FROM Ax=y
%*****
    V1=V_1_sort*D_1_root;  V2=V_2_sort*D_2_root;
    A=[-V_1_sort, V_2_sort; V1, V2];
    y=c_0*[V_1_sort(:,M); D_1_root(M,M)*V_1_sort(:,M)];  x=inv(A)*y;
    for r=1:1:M
        a(r)=x(r);
    end
    a_ref=transpose(a);
    for r=M+1:1:2*M
        b(r-M)=x(r);
    end
    b_trans=transpose(b);  c=zeros(M,1); c(M)=c_0;
    for k=1:1:length(index1)
        a_1(k)=a(index1(k));
    end
    a1=transpose(a_1);
    for k=1:1:length(index1)
        c_1(k)=c(index1(k));
    end
    c1=transpose(c_1);
    for k=1:1:length(index2)
        b_1(k)=b(index2(k));
    end
    b1=transpose(b_1);
%*****
%FIGURES: location of eigenvalues and eigenvectors
%*****
figure(1);
    plot (x1_real, x1_imaginary, '*', 'Color', 'r');
    xlabel('Re(lambda)', 'FontSize', 12);
    ylabel('Im(lambda)', 'FontSize', 12);
    title('Position of Complex Eigenvalues lambda', 'FontSize', 12);
figure(2);
    plot (x2_real, x2_imaginary, '*', 'Color', 'r');
    xlabel('Re(lambda)', 'FontSize', 12);
    ylabel('Im(lambda)', 'FontSize', 12);
    title('Position of Complex Eigenvalues lambda', 'FontSize', 12);

```

```
%for Delta_0=0.1 ONLY
figure(3);plot(xi, real(V_1_sort(:, 1)));
    xlabel('xi', 'FontSize', 12);
figure(4);plot(xi, real(V_1_sort(:, 3)));
    xlabel('xi', 'FontSize', 12);
figure(5);plot(xi, real(V_1_sort(:, 6))
    xlabel('xi', 'FontSize', 12);
figure(6);plot(xi, real(V_1_sort(:, 7)));
    xlabel('xi', 'FontSize', 12);
figure(7);plot(xi, real(V_1_sort(:, 9)));
    xlabel('xi', 'FontSize', 12);
figure(8);plot(xi, real(V_1_sort(:, 11)));
    xlabel('xi', 'FontSize', 12);
%*****
%THE END
%*****
```

Bibliography

- [1] Z.S. Agranovich and V.A. Marchenko, *The inverse problem of scattering theory*, Gordon and Breach Ltd., London, England, 1963.
- [2] G. Agrawal, *Nonlinear fiber optics*, Academic Press, San Diego, CA., 2001.
- [3] J.P. Berenger, *A perfectly matched layer for the absorption of electromagnetic waves*, Journal of Comp. Physics **114** (1994), 185–200.
- [4] ———, *Perfectly matched layer for the ftd solution of wave-structure interaction problems*, IEEE Transactions on Antennas and Propagation **44** (1996), 110–117.
- [5] W.C. Chew, J.M. Jin, and E. Michielssen, *Complex coordinate system as a generalized absorbing boundary condition*, IEEE **107** (1997), 2060–2063.
- [6] J.L. Davis, *Wave propagation in electromagnetic media*, Springer-Verlag, New York, NY., 1990.
- [7] B. Engquist and A. Majda, *Absorbing boundary conditions for the finite-difference approximation of the time-domain electromagnetic field equations*, IEEE Electromagn. Comput. **23** (1981), 377–382.
- [8] J. Fang, *Generalized perfectly matched layer for the absorption of propagating and evanescent waves in lossless and lossy material*, IEEE Transactions on Microwave Theory and Techniques **44** (1996), 2216–2222.

- [9] G.B. Folland, *Fourier analysis and its applications*, Brooks/Cole, Pacific Grove, CA., 1992.
- [10] W.P. Gribbons, M.A. Pinello and C. Cangellaris, *A stretched coordinate technique for numerical absorption of evanescent and propagating waves in planar waveguide structures*, IEEE Transactions on Microwave Theory and Techniques **43** (1995), 2883–2889.
- [11] S.L. Harris and R.J. Schilling, *Applied numeric methods*, Brooks/Cole, Pacific Grove, CA., 1999.
- [12] R. Higdon, *Numerical absorbing conditions for the wave equation*, Math. Comput. **49** (1987), 65–90.
- [13] P.D. Hislop and I.M. Sigal, *Introduction to spectral theory: With applications to schrodinger operators*, Springer-Verlag, New York, NY., 1996.
- [14] R. Holland and J. Williams, *Total-field versus scattered field finite-difference: A comparative assessment*, IEEE Nucl. Sci. **31** (1977), 629–651.
- [15] W.P. Huang, C.L. Xu, and K. Yokoyama, *Perfectly matched layer boundary condition for modal analysis of optical waveguides: leaky mode calculations*, IEEE Photonics Technology Letters **8** (1996), 652–654.
- [16] L.D. Landau and E.M. Lifshitz, *Quantum mechanics: Non-relativistic theory*, Pergamon Press Ltd., Oxford, Eng., 1977.
- [17] L.M. Magid, *Electromagnetic fields, energy, and waves*, John Wiley and Sons, Inc., New York, NY., 1972.
- [18] W.H. Press, Teukolsky S.A., W.T. Vetterling, and B.P. Flannery, *Numeical recipes, 2nd ed.*, Cambridge University Press, Cambridge, Eng., 1992.

- [19] C.M. Rappaport, *Perfectly matched absorbing boundary conditions based on anisotropic lossy mapping of space*, IEEE Microwave and Guided Wave Letters **5** (1995), 90–92.
- [20] Y. Rickard, *Improved absorbing boundary conditions for the time-domain methods in electromagnetics*, Ph.D Thesis, McMaster University, 2002.
- [21] H.H. Skilling, *Fundamentals of electric waves*, John Wiley and Sons, Inc., New York, NY., 1948.
- [22] J.A. Stratton, *Electromagnetic theory*, McGraw-Hill Book Company, Inc., New York, NY., 1941.
- [23] A. Taflov, *Review of the formulation and applications of the finite-difference time-domain method for numerical modelling of electromagnetic wave interactions with arbitrary structures*, Wave Motion **10** (1988), 547–582.
- [24] National Communications System Technology and Standards Division, *Telecommunications: Glossary of telecommunication terms*, General Services Administration Information Technology Service, 1996.
- [25] C.C. Weng and W.H. Weedon, *A 3d perfectly matched medium from modified maxwell's equations with stretched coordinates*, Microwave and Optical Technology Letters **7** (1994), 599–603.
- [26] K. S. Yee, *Numerical solution of initial boundary value problems involving maxwell's equation in isotropic media*, IEEE Trans. Antennas Propag. **AP-14** (1966), 302–307.
- [27] D. Zhou, W.P. Huang, D.G. Fang, and B. Chen, *The perfectly matched layer boundary condition for scalar finite-difference time-domain method*, IEEE Photonics Technology Letters **13** (2001), 454–456.